

1 **SUMMARY**

2
3
4 3 Widespread quorum-sensing (QS) enables bacteria to communicate and plays a critical role in
5
6 4 controlling bacterial virulence. However, effects of promiscuous QS crosstalk and its
7
8 5 implications for gene regulation and cell decision-making remain largely unknown. Here we
9
10 6 systematically studied the crosstalk between LuxR/I and LasR/I systems and found that QS
11
12 7 crosstalk can be dissected into signal crosstalk and promoter crosstalk. Further investigations
13
14 8 using synthetic positive feedback circuits revealed that signal crosstalk significantly decreases
15
16 9 circuit's bistable potential while maintaining unimodality. Promoter crosstalk, however,
17
18 10 reproducibly generates complex trimodal responses resulting from noise-induced state
19
20 11 transitions and host-circuit interactions. A mathematical model that integrates the circuit's
21
22 12 nonlinearity, stochasticity, and host-circuit interactions was developed, and its predictions of
23
24 13 conditions for trimodality were verified experimentally. Combining synthetic biology and
25
26 14 mathematical modeling, this work sheds light on the complex behaviors emerging from QS
27
28 15 crosstalk, which could be exploited for therapeutics and biotechnology.
29
30

1 **INTRODUCTION**

2 Quorum-sensing (QS) is a widespread mechanism bacteria use to regulate gene expression
3 and coordinate population behavior based on local cell density (Ng and Bassler, 2009). It is
4 achieved through the binding of QS regulators with their cognate signal molecules
5 (autoinducers) to regulate downstream QS pathways. Autoinducers are produced inside the
6 cell and diffuse into and out of bacterial cells. Therefore, an autoinducer’s intracellular
7 concentration correlates with local cell density (Ng and Bassler, 2009). There are diverse QS
8 mechanisms allowing for bacterial communication: gram-positive bacteria generally use
9 two-component systems mediated by peptides, while gram-negative bacteria primarily use
10 LuxR/LuxI-type systems mediated by acylated homoserine lactones (AHL) (Miller and
11 Bassler, 2001; Ng and Bassler, 2009). Many bacterial activities are controlled or regulated by
12 QS, such as antibiotic production, biofilm development, bioluminescence, colonization,
13 sporulation, symbiosis, and virulence (Jayaraman and Wood, 2008; LaSarre and Federle, 2013;
14 Miller and Bassler, 2001; Ng and Bassler, 2009; Solano et al., 2014).

15 With well-defined and characterized biological properties, several QS regulators and
16 corresponding autoinducers have also been used for synthetic gene networks. For example,
17 LuxR/LuxI and/or LasR/LasI pairs were used to generate programmed patterns (Basu et al.,
18 2005; Payne et al., 2013), trigger biofilm formation (Hong et al., 2012; Kobayashi et al.,
19 2004), develop synthetic ecosystems and program population dynamics (Balagadde et al.,
20 2008; Brenner et al., 2007), and construct synchronized oscillators (Danino et al., 2010;
21 Prindle et al., 2012), edge detectors (Tabor et al., 2009), and pulse generators (Basu et al.,
22 2004). RhIR/RhII has also been used in the study of generic mechanisms of natural selection
23 (Chuang et al., 2009) as well as for carrying out biological computations as chemical ‘wires’
24 (Tamsir et al., 2011).

25 However, effects of QS crosstalk, functional interactions between QS components that are
26 not naturally paired, remain unexplored. For example, widely used LuxR-family regulators
27 share extensive homologies and structural similarities in their corresponding autoinducers.
28 LuxR binds its natural ligand 3-oxo-C6-HSL (3OC6HSL, hereafter denoted as C6) to activate
29 the pLux promoter, while LasR bind 3-oxo-C12-HSL (3OC12HSL, hereafter denoted as C12)

1 to activate pLas (Table S1) (Fuqua et al., 1996; Meighen, 1994; Miller and Bassler, 2001; Ng
2 and Bassler, 2009; Schuster et al., 2004; Stevens and Greenberg, 1997). However, the LuxR
3 protein can also bind other HSLs, such as C7HSL and 3OC8HSL (Canton et al., 2008). When
4 binding C12, LasR is able to activate pLux in addition to the naturally paired pLas promoter
5 (Balagadde et al., 2008). Implications of such crosstalk on gene regulation and cell response
6 remain largely unknown.

7 Here, we use rationally designed gene networks to probe crosstalk between the LuxR/I and
8 LasR/I systems and investigate their elicited bistable behaviors from positive feedback
9 topologies. By using a synthetic biology approach, all combinations of autoinducer, regulator,
10 and promoter were tested to show that QS crosstalk can be dissected into signal crosstalk and
11 promoter crosstalk. When studied in the context of a synthetic positive feedback gene network,
12 our results indicate that QS crosstalk leads to distinct dynamic behaviors: signal crosstalk
13 significantly decreases the circuit's induction range for bistability, but promoter crosstalk
14 causes transposon insertions into the regulator gene and yields trimodal responses due to a
15 combination of mutagenesis and noise induced state transitions. To fully understand this
16 complex response, we developed and experimentally verified a mathematical model that takes
17 into account all of these factors to simulate and predict how varying the transposition rate can
18 modulate this trimodality. This reveals a novel factor of host-circuit interactions in shaping
19 complex responses of synthetic gene networks.

21 **RESULTS**

22 **Dissecting the crosstalk between LuxR/I and LasR/I using synthetic circuits.**

23 To characterize possible crosstalk between LuxR/I and LasR/I signaling systems, four
24 synthetic circuits, CP (constitutive promoter)-LuxR-pLux (Figure 1A), CP-LasR-pLux
25 (Figure 1B), CP-LasR-pLas (Figure S1A), and CP-LuxR-pLas (Figure S1B), were first built
26 to test all autoinducer-regulator-promoter combinations' impact on gene expression activation.
27 C6 and C12 were applied independently to all constructs, and green fluorescent protein (GFP)
28 expression under the regulation of pLux or pLas was measured as the readout.

29 It can be seen in Figure 1A that in addition to its natural partner C6, LuxR can also bind

1 with C12 molecules to activate pLux, which suggests that the binding with C6 or C12 results
2 in a similar conformational change of LuxR and therefore its activating functions remain
3 uninterrupted. Such an activation of a natural QS regulator-promoter pair by a cross-talking
4 autoinducer is here termed signal crosstalk. It can be seen that this signal crosstalk can fully
5 activate the system with comparable induction dosages. However, similar tests of signal
6 crosstalk of C6 with the Las regulator-promoter pair (Figure S1A) only show comparable
7 induction when the autoinducer concentration is as high as 10^{-3} M. This suggests that the
8 efficacy of signal crosstalk is QS system specific.

9 In addition to promiscuous autoinducer binding resulting in signal crosstalk, the systems
10 studied also displayed crosstalk between regulators and promoters, here termed promoter
11 crosstalk. It is shown in Figure 1B that, in addition to being able to activate pLas, LasR
12 significantly activates pLux when induced with its natural cognate ligand C12, though not
13 with C6, which suggests that LasR's DNA binding domain can recognize both pLas and pLux
14 when bound with its natural partner. This promoter crosstalk is robust over a wide range of
15 autoinducer concentrations. Similar tests of promoter crosstalk of C6-LuxR to pLas (Figure
16 S1B) show only weak induction. This suggests that the efficacy of promoter crosstalk is also
17 QS system specific. It should also be noted that a third type of crosstalk, regulator crosstalk,
18 in which naturally paired autoinducer and promoter function through a cross-talking regulator
19 protein, only exhibited minimal levels of activation (gray bar in Figure 1B and black bar in
20 Figure S1B).

21 To further verify the crosstalk under physiologically relevant dosages of autoinducers,
22 synthase genes LuxI and LasI were introduced to replace commercial chemicals in eight
23 different circuits (Figure S1C and 1D). The results further confirm that pLux can be activated
24 by LuxR with LuxI or LasI, as well as by LasR with LasI. This is consistent with the results
25 using commercial chemicals, indicating the crosstalk categorization is also applicable *in vivo*.
26 All combinatorial activations between LuxR/I and LasR/I systems are summarized in Figure
27 1C, with crosstalk highlighted in red. Taken together, detectable crosstalk between LuxR/I and
28 LasR/I systems can be categorized into two types: LasI (C12) can crosstalk with the LuxR
29 protein to induce pLux transcription (signal crosstalk), and the LasR-LasI (C12) complex can
30 also crosstalk with and activate the pLux promoter (promoter crosstalk).

Signal crosstalk induces distinct responses from positive feedback circuits.

Next, synthetic positive feedback circuits were constructed to investigate the impact of QS crosstalk in the context of gene regulatory networks. It is shown that the core of many bacteria's QS decision-making circuits is a positive feedback motif (Ji et al., 1995; Kaplan and Greenberg, 1985; de Kievit and Iglewski, 2000; Pestova et al., 1996; Piper et al., 1993; Seed et al., 1995). Because of its potential bistability, such a topology enables the bacteria to make appropriate binary decisions in response to changing environments (Ozbudak et al., 2004; Xiong and Ferrell, 2003; Guido et al., 2006; Isaacs et al., 2003). Synthetic positive feedback circuits serve as suitable platforms to probe the effects of signal and promoter crosstalk within the framework of gene regulatory networks.

The design shown in Figure 2A was first constructed to study signal crosstalk. In this circuit, expression of LuxR is regulated by the promoter pLux, which can be activated by LuxR when induced, forming a positive feedback loop. pLux driven GFP expression serves as the readout for LuxR levels. Robustness of history-dependent responses (hysteresis), a hallmark of many positive feedback topologies, is used as the main measure of signal crosstalk impacts as it captures the effectiveness of the circuit's decision-making functionality (Acar et al., 2005; Gardner et al., 2000; Wu et al., 2013).

As a benchmark, uninduced (Initial OFF) cells with the circuit were first induced with different concentrations of LuxR's natural inducer C6 and measured using flow cytometry (Figure 2B, blue). It can be seen that GFP is only turned on with 10^{-8} M or higher C6 induction. The cells treated with 10^{-4} M C6 (Initial ON) were then collected and diluted into new medium with the same concentrations of C6 (Figure 2B, red). These cells keep high GFP expression even with low C6 inductions (below 10^{-9} M) due to the self-sustaining nature of positive feedback loops. Taken together, these results illustrate this circuit's hysteretic response with C6 inducer concentrations between 0 and 10^{-8} M. This indicates that under C6 induction the positive feedback circuit is bistable between 0 and 10^{-8} M C6 induction. However, no bimodal distribution was observed within the bistable region based on flow cytometry measurements (Figure 2D, purple and light purple; and Figure S2A), suggesting that the barrier between the two states is too high for inherent gene expression stochasticity to

1 overcome (Acar et al., 2005; Gardner et al., 2000).

2 Next, C12 was used to induce the same construct to investigate the impact of signal
3 crosstalk on gene network regulation. Similar induction experiments were carried out and the
4 results are shown in Figure 2C. It can be seen that this circuit also displays hysteresis, but
5 with a much smaller bistable region between 10^{-8} and 10^{-6} M C12. Flow cytometry results
6 within the bistable region also show no bimodal distributions (Figure 2D, cyan and light cyan;
7 and Figure S2B).

8 To quantitatively understand the signal crosstalk caused shrinkage of the bistable region, an
9 ordinary differential equation (ODE) model of LuxR-pLux auto-activation was developed.
10 Two major kinetic events, LuxR transcription and translation, are described by two ODEs
11 with all binding between chemical species incorporated into model terms. After fitting the
12 parameters using existing literature and experimental measurements (Table S2), the model can
13 capture the experimental results (lines in Figure 2B and 2C) with accuracy. Inspection of
14 model parameters reveals that the bistable region decrease caused by signal crosstalk can be
15 largely accounted for by differential binding affinities between LuxR and C6 and C12. This
16 suggests a new way to perturb QS decision-making through utilization of crosstalking
17 autoinducers, which could be useful for clinical therapies.

19 **Promoter crosstalk induces unexpected and complex bimodal responses.**

20 To study the impacts of promoter crosstalk, a positive feedback circuit was constructed with
21 LasR under the regulation of pLux (Figure 3A). It is shown in Figure 1B that LasR can
22 activate pLux when induced by C12. Therefore this circuit also forms a positive feedback
23 loop in the presence of C12. GFP under regulation of pLux is again included as a readout for
24 LasR. Experimental explorations of hysteresis were carried out and the results are shown in
25 Figure 3B. It can be seen that initial OFF cells (blue) exhibit a non-monotonic response to
26 C12 induction: GFP expression increases with C12 concentration, but begins to uniformly
27 decrease when C12 induction exceeds 10^{-8} M (Figure 3B, and Figure S3A and 3B). Cells
28 induced with 10^{-4} M C12 were then collected and diluted into fresh medium with the same
29 inducer concentrations as the initial OFF cells. Flow cytometry data show that all samples
30 exhibit unimodal minimal fluorescence signals that are even lower than the basal GFP

1 expression of initial OFF cells (Figure 3B and 3C green, and Figure S3B).

2 Considering that both C12 and exogenous gene overexpression may be toxic to cells, as
3 well as the fact that initial OFF cells can be turned on with lower induction dosages, cells
4 induced with lower than 10^{-4} M but higher than 10^{-10} M C12 were collected as new initial ON
5 cells to further explore possible hysteresis of this circuit. Collected cells were diluted into
6 fresh medium with the same concentrations of C12. These new initial ON cells demonstrate
7 the same expression pattern as the initial OFF cells when grown in inducer concentrations
8 from 0 to 10^{-9} M, but they show much lower fluorescence values at higher concentrations. For
9 example, the red points in Figure 3B illustrate the GFP average of 10^{-9} M induced initial ON
10 cells when collected and re-diluted into a range of C12 concentrations (See Figure S3C for
11 results with other initial induction dosages). Examination of the flow cytometry
12 measurements of these ON cells reveals that bimodal distributions emerge within the
13 concentration range of 10^{-8} M to 10^{-4} M C12. Interestingly, one peak of the distribution is at
14 the high state and the other is at the minimal expression state, even lower than basal
15 expression (Figure 3C, red). So unlike classic bimodal responses due to bistability,
16 LasR-pLux positive feedback exhibits bimodality with the lower peak's expression even
17 weaker than the OFF state. To exclude the possibility that this bimodality is triggered by
18 inherent properties of the LasR-C12 complex, similar hysteresis experiments were carried out
19 for the linear CP-LasR-pLux circuit (Figure 1B). Results show that the initial OFF and ON
20 cells both exhibit unimodal expression without hysteresis (Figure S3D). The bimodality is,
21 therefore, unique to the initial ON cells with LasR-pLux positive feedback.

22 23 **Bimodality results from circuit-host interactions.**

24 The remaining question is: what is the cause of the minimal expression state? To resolve this
25 problem, new initial ON samples at concentrations of 10^{-11} M to 10^{-4} M C12 (Figure 3B, red
26 triangles) were collected. Their plasmids were extracted and digested for genotyping. The
27 agarose gel electrophoresis results show that a new band (~3.2 kb) replaces the original
28 fragment band (wild type, ~1.9 kb) for samples in 10^{-8} ~ 10^{-4} M C12, and that a faint
29 original-fragment band can also be seen for samples with 10^{-8} and 10^{-7} M C12 inductions
30 (Figure 3D). Further sequencing analyses verify that an IS10 transposase is inserted into the

1 LasR gene at the 682 bp site and this insertion is flanked by two 9 bp direct repeats
2 5'-CGCGTAGCG-3' (Figure 3D and Supplementary Information), which is consistent with
3 reported hotspots for IS10 insertion (Kovarík et al., 2001).

4 The insertion abolishes LasR's ability to activate downstream GFP expression, which in
5 turn causes the cells' fluorescence signal to be even weaker than basal expression when LasR
6 is intact. Cells with this type of mutation form the low GFP peak in the bimodal distributions
7 in Figure 3C. On the other hand, cells that do not mutate are able to maintain a high GFP
8 expression due to positive feedback, forming the GFP ON peak of the bimodal distributions.
9 Taken together, the combination of gene network activated GFP expression and mutation
10 caused GFP inhibition drive the emergence of a bimodal distribution.

11 **Trimodality predicted by expanded model.**

12 In light of the verified mutation in the LasR-pLux positive feedback system, the mathematical
13 model was expanded to take into account crosstalk triggered genetic changes to better
14 describe the circuit. To enable comparison with flow cytometry results, the ODEs were
15 transformed into corresponding biochemical reactions and simulated stochastically (Gillespie,
16 1977). In addition, each cell was assigned a probability of mutation throughout the simulation
17 (Figure 4C inset), which is dependent on the cell's current LasR/GFP level and the
18 transposition rate. Once mutated, the cells had only minimal GFP expression strength and
19 remained mutated until the end of the simulation. Finally, growth rate differences between
20 wild type and mutated cells were computed from experiments (Figure S4A) and taken into
21 consideration in the simulation. Results of stochastic simulations of this expanded model are
22 shown in Figure 4A, exhibiting the bimodal distribution observed experimentally (red curves
23 in Figure. 4A, simulation; and 4B, experiment).

24 To further investigate the impact of this mutation on the circuit's functions, simulations
25 were carried out with perturbed parameters to mimic various scenarios. First, the transposition
26 rate was artificially set to zero, and the simulations show that the system can also exhibit a
27 bimodal distribution (Figure 4A, blue), with the OFF peak exhibiting basal GFP expression.
28 Bimodality has been reported to arise from stochastic state switching of a bistable system
29 without any genetic changes (Acar et al., 2005; Gardner et al., 2000; Tan et al., 2009). The
30

1 same mechanism leads to simulated bimodality of this LasR-pLux circuit when there is no
2 mutation.

3 While it is almost impossible to eliminate mutation, it is possible to decrease the
4 transposition rate experimentally. To explore the impacts of mutation in a more realistic
5 scenario, simulations were carried out with positive but smaller transposition rates.
6 Interestingly, the system demonstrates a trimodal distribution (Figure 4A, green). In this
7 distribution, there are three groups of cells: ON, OFF, and Mutated. Those cells initialized at
8 the ON state freely transition to and from the OFF state, due to the system's bistability.
9 Meanwhile, all cells have the chance to mutate and stay mutated (Figure 4C). Given enough
10 time and the right measurement window, all three groups of cells would be visible. Within this
11 window, the portion of ON and OFF cells will gradually decrease and the number of mutated
12 cells will increase because the mutation is irreversible. The effect of a decreased transposition
13 rate is essentially slowing down the ON to Mutation transition rate and giving enough time
14 for ON to OFF transitions and hence the emergence of the OFF peak. Time courses of the
15 simulations demonstrate gradual emergence and evolution of these three populations of cells
16 (Figure 4D).

18 **Experimental validation of trimodal responses by lowering growth temperature.**

19 Previous reports indicated that transposition frequency can be perturbed by growth
20 temperatures (McClintock, 1984; Ohtsubo et al., 2005; Sousa et al., 2013). To tune the
21 transposition rate, experiments were carried out with cells cultured at a lower 34 °C
22 temperature, which was shown to slow down crosstalk triggered mutation of this circuit
23 (Figure S4B). Consistent with model predictions, initial ON cells induced with 10^{-8} M C12
24 exhibited a trimodal response when the growth temperature was tuned from 37 °C to 34 °C
25 (Figure 4B, green). Moreover, temporal evolution of the proportion of each subpopulation
26 was consistent with model predictions: the portion of ON cells gradually decreased, the
27 Mutation portion increased, and the OFF portion increased first and then decreased as time
28 went on (Figure 4E). Growth rates of cells at Mutated, ON, or OFF states were also measured
29 and show no difference when cultured at these two different temperatures (Figure S4A). The
30 emergence of the OFF peak, therefore, is fully accounted for by the decrease of transposition

1 rate, which slows down the direct transitions from ON to Mutation and therefore gives the
2 cells time to layover at the OFF state. This is also evidenced by the smaller portion of
3 Mutated cells when grown at 34 °C compared with 37 °C (Figure S4B).

4 Furthermore, a microfluidic platform coupled with time-lapse imaging was also employed
5 to verify model predictions (Ferry et al., 2011). Cells were pretreated with 10^{-9} M C12 until
6 steady state as the initial ON cells before being loaded into the device and induced with 10^{-8}
7 M C12 at 34 °C to mimic the experimental protocols used in Figure 4E. Initially, there was
8 only one ON cell loaded into the trap (Figure 5A and Movie S1). At the 8th hour, it can be seen
9 that two populations began to emerge: some cells became OFF and some stayed ON.
10 Mutations started to occur shortly after the 8th hour, and the OFF and Mutation cells
11 accounted for around 90 percent of the population after 16 hours. Eventually mutation state
12 cells took up the majority of the population. There also existed several OFF cells which
13 became ON again, owing to stochastic gene expression noise, but they eventually exhibit a
14 similar evolving process: ON to OFF or Mutation (Figure 5B and Movie S1), which is
15 consistent with the stochastic model simulations shown in Figure 4C.

16 Altogether, the flow cytometry and microfluidic data confirmed the model's predicted
17 trimodality, which arises from bistability of the positive feedback circuit and host-circuit
18 interactions. In the context of positive feedback, cells transition freely between the ON and
19 OFF states, but it is easier for ON state cells to transition to the OFF state because of the
20 asymmetric energy barrier (Figure S4C). However, the ON cells can also transition to the
21 Mutated state, which carries an advantage of growth rate (Figure S4A). Compared to OFF
22 state cells, those in the ON state would transition more frequently to the Mutated state at
23 37 °C, leading to the bimodal distribution (Figure 3). When the growth temperature is reduced
24 to 34 °C, the transposition frequency also decreases, meaning that the barrier between ON and
25 Mutated state increases. Therefore, more ON cells would transition to the OFF state, which
26 promotes the emergence of trimodality (Figure 5C).

27 28 **DISCUSSION**

29 QS is a ubiquitous mechanism in nature, and its regulator-autoinducer pairs, such as

1 LuxR/LuxI and LasR/LasI, have been used in synthetic biology for a wide range of
2 applications (Balagadde et al., 2008; Basu et al., 2004, 2005; Brenner et al., 2007; Chen et al.,
3 2014; Chuang et al., 2009; Danino et al., 2010; Hong et al., 2012; Kobayashi et al., 2004;
4 Payne et al., 2013; Prindle et al., 2012; Tabor et al., 2009; Tamsir et al., 2011; Pai et al., 2012).
5 However, evolutionary pressures from limited resources in a competitive environment
6 promote promiscuous bacterial communication, which takes the form of either different
7 genera of bacteria producing the same types of autoinducers or non-specific
8 regulator-autoinducer binding (Balagadde et al., 2008; Gray et al., 1994; Hong et al., 2012;
9 Miller and Bassler, 2001; Pérez et al., 2011; Winzer et al., 2000). As a result, QS
10 regulator-autoinducer pairs are not orthogonal, and there is crosstalk between them.
11 Dissecting the crosstalk is critical for unraveling the underlying principles of bacterial
12 decision-making and survival strategies for both natural and synthetic systems.

13 In this work, we used synthetic biology approaches to dissect QS crosstalk between LuxR/I
14 and LasR/I. By applying engineering principles to construct modular gene networks, we were
15 able to characterize and categorize QS crosstalk into signal crosstalk, where LuxR binds with
16 the non-naturally paired C12 to activate pLux, and promoter crosstalk, where LasR binds with
17 C12 to activate non-naturally paired pLux. However, regulator crosstalk, in which the
18 naturally paired autoinducer and promoter function through a cross-talking regulator protein,
19 was not detected in this work.

20 When signal crosstalk is constructed and tested in the context of positive feedback, our
21 results showed a significant shrinkage of the bistable region. Because of this topology's
22 bistable capability and wide presence in most bacterial QS decision-making circuits, such a
23 decrease in bistability robustness due to QS crosstalk suggests a new strategy for developing
24 anti-infection therapeutics. Namely, we might exploit "artificial" crosstalk to disrupt
25 intercellular communication specificity and collapse the group's coordination, which could be
26 an efficient and economic approach in medical treatments, especially for QS-dependent
27 bacterial infection.

28 On the other hand, promoter crosstalk caused complex trimodal responses when embedded
29 within a positive feedback circuit. This can only be explained when network bistability, gene
30 expression stochasticity, and genetic mutations are all taken into consideration. These results

1 highlight the potential for engineering gene networks to express complex behaviors due to
2 host-circuit interactions. We computationally predicted and experimentally verified that the
3 C12-LasR-pLux positive feedback circuit could drive the formation of three subpopulations
4 from an isogenic initial culture: one population expressing high GFP expression, the second
5 showing basal GFP expression, and the third population with no GFP expression. The high
6 and low GFP states are the result of positive feedback enabled bistability and gene expression
7 stochasticity-induced random state transitions: commonly reported as a hallmark of many
8 bistable systems (Acar et al., 2005; Gardner et al., 2000; Tan et al., 2009; Guido et al., 2006;
9 Isaacs et al., 2003). This population heterogeneity is not caused by genetic factors.

10 The third non-GFP population is the result of genetic mutation from IS10 insertion. The
11 mutation only happened in the C12-LasR-pLux positive feedback circuit but not in
12 CP-LasR-pLux-C12 (Figure S 3D) or the C12-LuxR-pLux positive feedback circuit (Figure S
13 2B). It is, therefore, possible that the special sequence arrangements of the positive feedback
14 circuit (for example, the symmetric pLux promoters flanking the LasR gene) on the plasmid
15 coupled with the stress of exogenous protein overexpression led to transposon activation and
16 gene network destruction. Given that many current synthetic gene circuits are constructed
17 with a similar symmetric structure in a plasmid (such as Promoter-RBS-Gene1-RBS-Gene2-,
18 or Promoter-RBS-Gene1-Terminator-Promoter-RBS-Gene2-Terminator), the mutation may
19 occur for a wide range of engineered gene circuits. On the other hand, from an engineer's
20 perspective, the mutation stands in contrast to previously reported host-circuit interactions,
21 which are primarily related to resource limitation and resulting growth defects (Brophy and
22 Voigt, 2014). Here we were able to illustrate that both the components used and the topology
23 of the network constructed could contribute to resource independent host-circuit interactions.
24 This concept of combining nonlinear dynamics and host-circuit interactions to enrich
25 population diversity expands our understanding of mechanisms contributing to cell-cell
26 variability, and suggests new directions in engineering gene networks to utilize hybrid factors.

27 Taken together, our studies not only showcase living cells' amazing complexity and the
28 difficulty in the refining of engineered biological systems, but also reveal an overlooked
29 mechanism by which multimodality arises from the combination of an engineered gene circuit
30 and host-circuit interactions (Ellis et al., 2009; Hussain et al., 2014; Litcofsky et al., 2012;

1 Nevozhay et al., 2013; Prindle et al., 2014).

3 **SIGNIFICANCE**

4 **Widespread quorum-sensing (QS) enables bacteria to communicate and plays a critical**
5 **role in controlling bacterial virulence. QS components have also been widely used in**
6 **synthetic biology applications. However, effects of promiscuous QS crosstalk remain**
7 **unexplored. Here we systematically studied the crosstalk between LuxR/I and LasR/I**
8 **systems. Combining synthetic biology and mathematical modeling, this work reveals the**
9 **complexity of QS crosstalk, which is critical for unraveling the underlying principles of**
10 **bacterial decision-making and survival strategies for both natural and synthetic systems.**
11 **Furthermore, the unusual hybrid multimodality arising from the combination of**
12 **engineered gene circuits and circuit-host interactions could be utilized in biotechnology.**

14 **EXPERIMENTAL PROCEDURES**

15 **Strains, Growth Conditions and Media**

16 All cloning experiments were performed in *E.coli* DH10B (Invitrogen, USA), and
17 measurements of positive feedback response were conducted in DH10B and MG1655. Cells
18 were grown at 37 °C (unless specified) in liquid and solid Luria-Bertani (LB) broth medium
19 with 100 µg/mL ampicillin. Chemical 3OC6HSL and 3OC12HSL (Sigma-Aldrich, USA)
20 were dissolved in ddH₂O and DMSO, respectively. Cultures were shaken in 5 mL or 15 mL
21 tubes at 220 rotations per minute (r.p.m), and inducers were added at OD₆₀₀~0.1.

23 **Plasmids Construction**

24 Plasmids were constructed according to standard molecular cloning protocols and the genetic
25 circuits were assembled using standardized BioBricks methods based on primary modules
26 (Table S4) from the iGEM Registry (www.parts.igem.org). The receiver CP-LuxR-pLux was
27 constructed from six BioBrick standard biological parts: BBa_K176009 (Constitutive
28 promoter, CP), BBa_B0034 (Ribosome binding site, RBS), BBa_C0062 (luxR gene),
29 BBa_B0015 (transcriptional terminator), BBa_R0062 (lux promoter), and BBa_E0240 (GFP

1 generator, RBS-GFP-T). As an example, to produce the RBS-LuxR part, LuxR plasmid was
2 digested by *XbaI* and *PstI* to produce a fragment while the RBS plasmid was digested by *SpeI*
3 and *PstI* as the vector. The fragment and vector were purified by gel electrophoresis (1% TAE
4 agarose gel) and extracted using a PureLink gel extraction kit (Invitrogen). Then, the fragment
5 and vector were ligated together using T4 DNA ligase, the ligation products were transformed
6 into *E.coli* DH10B and clones were screened by plating on 100 µg/mL ampicillin LB agar
7 plates. Finally their plasmids were extracted and verified by double restriction digest (*EcoRI*
8 and *PstI*) and DNA sequencing (Biodesign sequencing lab in ASU). After confirming that the
9 newly assembled RBS-LuxR was correct, subsequent rounds to produce the
10 RBS-LuxR-Terminator were performed similarly until completing the entire receiver
11 CP-LuxR-pLux construction. All the other receivers and positive feedback circuits were
12 assembled similarly. Restriction enzymes and T4 DNA ligase were from New England
13 Biolabs. All the constructs were verified by sequencing step by step. To keep all the
14 constructs' expression consistent in the cell, we transferred all the fragments into the pSB1A3
15 vector before test.

17 **Flow Cytometry.**

18 All the samples were analyzed at the time points indicated on an Accuri C6 flow cytometer
19 (Becton Dickinson, USA) with 488 nm excitation and 530±15 nm emission detection (GFP).
20 The data were collected in a linear scale and noncellular low-scatter noise was removed by
21 thresholding. All measurements of gene expression were obtained from at least three
22 independent experiments. For each culture, 20,000 events were collected at a slow flow rate.
23 Data files were analyzed using MATLAB (MathWorks).

25 **Hysteresis Experiment**

26 For OFF→ON experiments, initially uninduced overnight culture was diluted into fresh media,
27 grown at 37 °C and 220 r.p.m for about 1.5 h (OD_{600} ~0.1), then distributed evenly into new
28 tubes and induced with various amounts of C6 or C12. Flow cytometry analyses were
29 performed at 6, 12, and 21 hours to monitor the fluorescence levels, which generally became
30 stable after 6 hours induction according to our experience. For ON→OFF experiments,

1 initially uninduced cells were induced with 10^{-4} M (or 10^{-9} M) autoinducer and tested by flow
2 cytometry to ensure they were fully induced. Cells were then collected with low-speed
3 centrifugation, washed twice, resuspended with fresh medium, and at last inoculated into
4 fresh medium with varying inducer concentrations at a 1:80 ratio. For the LasR-pLux positive
5 feedback system, we only diluted once and grew them for 6, 12, 18, 24, or 32 hours, but for
6 the other hysteresis experiments, the ON cells were collected and diluted twice into new
7 medium with the same concentrations of C6 or C12 at 12 h and 24 h.

9 **Growth Curve Assay**

10 First, different initial states cells were collected: initial OFF cells were cells grown overnight
11 without inducers, initial ON cells were initial OFF cells induced with 10^{-9} M C12 for 12 hours,
12 and the Mutated cells were cells induced with 10^{-4} M C12 for 12 hours, diluted into fresh
13 media with 10^{-4} M C12, and grown at 37 °C for another 12 h. Before the growth rate assay, all
14 the cells' fluorescence was tested by flow cytometry to verify their states. Growth rate was
15 measured by using absorbance at 600 nm with a plate reader (BioTek, USA). Cells from each
16 state were then diluted into fresh LB media (1000 μ L, O.D. \sim 0.06) with 10^{-8} M C12 and
17 grown at 37 or 34 °C. For each sample, OD was measured by using 200 μ L cultures in a
18 96-well plate and tested over 24 hours. The experiments were independently replicated three
19 times.

21 **Microfluidics, Fluorescence Microscopy, and Image Processing**

22 The use of microfluidic devices coupled with fluorescence measurement allowed us to
23 measure gene network dynamics in single cells. Media flow direction and speed was
24 controlled through hydrostatic pressure. A detailed description of the chip can be found in the
25 work of *Ferry MS, et al* (Ferry et al, 2011). Once the cell was loaded into the trap, the flow
26 was reversed and its rate was slowed to \sim 120 μ m/min to ensure that the cells would not be
27 washed away and would receive enough nutrients. Furthermore, care was taken to avoid
28 introducing bubbles to any part of the chip as they considerably disrupt flow. The chip
29 temperature was maintained at 34 °C with an external microscope stage (Tokai Hit, Japan).
30 Inducer concentrations were controlled by adjusting the heights of the inducer-containing

1 media syringes relative to one another.

2 Images were taken using a Nikon Eclipse Ti inverted microscope (Nikon, Japan) equipped
3 with an LED-based Lumencor SOLA SE Light Engine with the appropriate filter sets. The
4 excitation wavelength for GFP was 472 nm, and fluorescence emission was detected with a
5 Semrock 520/35 nm band pass filter. Phase and fluorescent images were taken under a
6 magnification of 40X, and perfect focus was maintained automatically using Nikon Elements
7 software.

8 Initially OFF cells (K-12 MG1655) induced with 10^{-9} M C12 (6 hours) were collected as
9 the initial ON cells, washed, resuspended with fresh media and then loaded into the trap. 100
10 $\mu\text{g/mL}$ ampicillin was added into media 1 and 2, but only media 2 was augmented with the
11 corresponding inducer (10^{-8} M C12). The microfluidic device was used to control the
12 chemical concentration by switching between media 1 and 2. For initial ON cells, media 2
13 was provided to the cells for the duration of the experiment. To prevent photobleaching and
14 phototoxicity to the cells in the trap, exposure time was limited to 100 ms for GFP.

15 Images were taken every 5 minutes for about 28 hours in total. The pixels in all images are
16 normalized to 0 – 1 range before analysis. One image was chosen for quantification every 15
17 minutes (i.e. three images). For each cell, the intensity was calculated by averaging three
18 selected points (left, middle, and right) in the cell and then subtracting the background. Since
19 all the cells are offspring of the first initial ON cell, each branch in Figure 5b stands for one
20 progeny. The cells that were washed away or had less than three generations were not
21 analyzed.

22
23 **Mathematical Modeling.** Ordinary differential equation models were solved and analyzed by
24 MATLAB. Stochastic simulations were written in MATLAB and run on a standard personal
25 computer (details are provided in Supplemental Information).

26 27 **SUPPLEMENTAL INFORMATION**

28 Supplemental Information contains full details about the mathematical modeling construction
29 and parameter fittings, five figures and four tables and can be found with this article online.

1 **AUTHOR CONTRIBUTIONS**

2 X.W. and F.W. designed the study; F.W. performed the experiments and carried out the
3 mathematical modeling; X.W. and F.W. analyzed the data; D.J.M. and F.W. made the
4 microfluidic chips; F.W, D.J.M., and X.W. wrote the manuscript.

6 **ACKNOWLEDGMENTS**

7 We thank Jeff Hasty for the microfluidic setup and chip design. We also thank Riqi Su and
8 Philippe Faucon for helpful discussions and suggestions. D.J.M is partially supported by ASU
9 IRA Fulton School of Engineering's Dean's fellowship. This study was financially supported
10 by National Science Foundation Grant DMS-1100309, American Heart Association Grant
11 11BGIA7440101, and National Institutes of Health Grant GM106081 (to X.W.).

13 **REFERENCES**

14 Acar, M., Becskei, A., and van Oudenaarden, A. (2005). Enhancement of cellular memory by
15 reducing stochastic transitions. *Nature* 435, 228 - 232.

16 Balagadde, F.K., Song, H., Ozaki, J., Collins, C.H., Barnet, M., Arnold, F.H., Quake, S.R., and
17 You, L. (2008). A synthetic Escherichia coli predator-prey ecosystem. *Mol Syst Biol* 4, 187.

18 Basu, S., Mehreja, R., Thiberge, S., Chen, M.-T., and Weiss, R. (2004). Spatiotemporal control of
19 gene expression with pulse-generating networks. *Proc. Natl. Acad. Sci. U. S. A.* 101, 6355 - 6360.

20 Basu, S., Gerchman, Y., Collins, C.H., Arnold, F.H., and Weiss, R. (2005). A synthetic
21 multicellular system for programmed pattern formation. *Nature* 434, 1130 - 1134.

22 Brenner, K., Karig, D.K., Weiss, R., and Arnold, F.H. (2007). Engineered bidirectional
23 communication mediates a consensus in a microbial biofilm consortium. *Proc. Natl. Acad. Sci. U.*
24 *S. A.* 104, 17300 - 17304.

25 Brophy, J.A.N., and Voigt, C.A. (2014). Principles of genetic circuit design. *Nat. Methods* 11, 508
26 - 520.

27 Canton, B., Labno, A., and Endy, D. (2008). Refinement and standardization of synthetic
28 biological parts and devices. *Nat Biotechnol* 26, 787 - 793.

29 Chen, A.Y., Deng, Z., Billings, A.N., Seker, U.O.S., Lu, M.Y., Citorik, R.J., Zakeri, B., and Lu,
30 T.K. (2014). Synthesis and patterning of tunable multiscale materials with engineered cells. *Nat.*
31 *Mater.* 13, 515 - 523.

- 1 Chuang, J.S., Rivoire, O., and Leibler, S. (2009). Simpson' s paradox in a synthetic microbial
2 system. *Science* 323, 272 - 275.
- 3 Danino, T., Mondragon-Palomino, O., Tsimring, L., and Hasty, J. (2010). A synchronized quorum
4 of genetic clocks. *Nature* 463, 326 - 330.
- 5 Ellis, T., Wang, X., and Collins, J.J. (2009). Diversity-based, model-guided construction of
6 synthetic gene networks with predicted functions. *Nat. Biotechnol.* 27, 465 - 471.
- 7 Ferry, M.S., Razinkov, I.A., and Hasty, J. (2011). Microfluidics for synthetic biology: from design
8 to execution. *Methods Enzym.* 497, 295 - 372.
- 9 Fuqua, C., Winans, S.C., and Greenberg, E.P. (1996). CENSUS AND CONSENSUS IN
10 BACTERIAL ECOSYSTEMS: The LuxR-LuxI Family of Quorum-Sensing Transcriptional
11 Regulators. *Annu. Rev. Microbiol.* 50, 727 - 751.
- 12 Gardner, T.S., Cantor, C.R., and Collins, J.J. (2000). Construction of a genetic toggle switch in
13 *Escherichia coli*. *Nature* 403, 339 - 342.
- 14 Gillespie, D. (1977). Exact stochastic simulation of coupled chemical reactions. *J Phys Chem* 81,
15 2340 - 2361.
- 16 Gray, K.M., Passador, L., Iglewski, B.H., and Greenberg, E.P. (1994). Interchangeability and
17 specificity of components from the quorum-sensing regulatory systems of *Vibrio fischeri* and
18 *Pseudomonas aeruginosa*. *J. Bacteriol.* 176, 3076 - 3080.
- 19 Guido, N.J., Wang, X., Adalsteinsson, D., McMillen, D., Hasty, J., Cantor, C.R., Elston, T.C., and
20 Collins, J.J. (2006). A bottom-up approach to gene regulation. *Nature* 439, 856 - 860.
- 21 Hong, S.H., Hegde, M., Kim, J., Wang, X., Jayaraman, A., and Wood, T.K. (2012). Synthetic
22 quorum-sensing circuit to control consortial biofilm formation and dispersal in a microfluidic
23 device. *Nat. Commun.* 3, 613.
- 24 Hussain, F., Gupta, C., Hirning, A.J., Ott, W., Matthews, K.S., Josić, K., and Bennett, M.R.
25 (2014). Engineered temperature compensation in a synthetic genetic clock. *Proc. Natl. Acad. Sci.*
26 201316298.
- 27 Isaacs, F.J., Hasty, J., Cantor, C.R., and Collins, J.J. (2003). Prediction and measurement of an
28 autoregulatory genetic module. *Proc. Natl. Acad. Sci.* 100, 7714 - 7719.
- 29 Jayaraman, A., and Wood, T.K. (2008). Bacterial quorum sensing: signals, circuits, and
30 implications for biofilms and disease. *Annu. Rev. Biomed. Eng.* 10, 145 - 167.
- 31 Ji, G., Beavis, R.C., and Novick, R.P. (1995). Cell density control of staphylococcal virulence
32 mediated by an octapeptide pheromone. *Proc. Natl. Acad. Sci. U. S. A.* 92, 12055 - 12059.
- 33 Kaplan, H.B., and Greenberg, E.P. (1985). Diffusion of autoinducer is involved in regulation of
34 the *Vibrio fischeri* luminescence system. *J. Bacteriol.* 163, 1210 - 1214.

- 1 De Kievit, T.R., and Iglewski, B.H. (2000). Bacterial quorum sensing in pathogenic relationships.
2 Infect. Immun. 68, 4839 - 4849.
- 3 Kobayashi, H., Kaern, M., Araki, M., Chung, K., Gardner, T.S., Cantor, C.R., and Collins, J.J.
4 (2004). Programmable cells: interfacing natural and engineered gene networks. Proc Natl Acad
5 Sci U A 101, 8414 - 8419.
- 6 Kovarik, A., Matzke, M.A., Matzke, A.J., and Koulaková, B. (2001). Transposition of IS10 from
7 the host Escherichia coli genome to a plasmid may lead to cloning artefacts. Mol. Genet.
8 Genomics MGG 266, 216 - 222.
- 9 LaSarre, B., and Federle, M.J. (2013). Exploiting Quorum Sensing To Confuse Bacterial
10 Pathogens. Microbiol. Mol. Biol. Rev. 77, 73 - 111.
- 11 Litcofsky, K.D., Afeyan, R.B., Krom, R.J., Khalil, A.S., and Collins, J.J. (2012). Iterative
12 plug-and-play methodology for constructing and modifying synthetic gene networks. Nat.
13 Methods 9, 1077 - 1080.
- 14 McClintock, B. (1984). The significance of responses of the genome to challenge. Science 226,
15 792 - 801.
- 16 Meighen, E.A. (1994). Genetics of Bacterial Bioluminescence. Annu. Rev. Genet. 28, 117 - 139.
- 17 Miller, M.B., and Bassler, B.L. (2001). Quorum Sensing in Bacteria. Annu. Rev. Microbiol. 55,
18 165 - 199.
- 19 Nevozhay, D., Zal, T., and Balazsi, G. (2013). Transferring a synthetic gene circuit from yeast to
20 mammalian cells. Nat. Commun. 4, 1451.
- 21 Ng, W.-L., and Bassler, B.L. (2009). Bacterial Quorum-Sensing Network Architectures. Annu.
22 Rev. Genet. 43, 197 - 222.
- 23 Ohtsubo, Y., Genka, H., Komatsu, H., Nagata, Y., and Tsuda, M. (2005).
24 High-temperature-induced transposition of insertion elements in burkholderia multivorans ATCC
25 17616. Appl. Environ. Microbiol. 71, 1822 - 1828.
- 26 Ozbudak, E.M., Thattai, M., Lim, H.N., Shraiman, B.I., and Van Oudenaarden, A. (2004).
27 Multistability in the lactose utilization network of Escherichia coli. Nature 427, 737 - 740.
- 28 Pai, A., Tanouchi, Y., and You, L. (2012). Optimality and robustness in quorum sensing
29 (QS)-mediated regulation of a costly public good enzyme. Proc. Natl. Acad. Sci. U. S. A. 109,
30 19810 - 19815.
- 31 Payne, S., Li, B., Cao, Y., Schaeffer, D., Ryser, M.D., and You, L. (2013). Temporal control of
32 self-organized pattern formation without morphogen gradients in bacteria. Mol. Syst. Biol. 9.
- 33 Pérez, P.D., Weiss, J.T., and Hagen, S.J. (2011). Noise and crosstalk in two quorum-sensing
34 inputs of Vibrio fischeri. BMC Syst. Biol. 5, 153.

- 1 Pestova, E.V., Håvarstein, L.S., and Morrison, D.A. (1996). Regulation of competence for genetic
2 transformation in *Streptococcus pneumoniae* by an auto-induced peptide pheromone and a
3 two-component regulatory system. *Mol. Microbiol.* *21*, 853 – 862.
- 4 Piper, K.R., Beck von Bodman, S., and Farrand, S.K. (1993). Conjugation factor of
5 *Agrobacterium tumefaciens* regulates Ti plasmid transfer by autoinduction. *Nature* *362*, 448 – 450.
- 6 Prindle, A., Samayoa, P., Razinkov, I., Danino, T., Tsimring, L.S., and Hasty, J. (2012). A sensing
7 array of radically coupled genetic *^*biopixels/’ . *Nature* *481*, 39 – 44.
- 8 Prindle, A., Selimkhanov, J., Li, H., Razinkov, I., Tsimring, L.S., and Hasty, J. (2014). Rapid and
9 tunable post-translational coupling of genetic circuits. *Nature* *508*, 387 – 391.
- 10 Schuster, M., Urbanowski, M.L., and Greenberg, E.P. (2004). Promoter specificity in
11 *Pseudomonas aeruginosa* quorum sensing revealed by DNA binding of purified LasR. *Proc. Natl.*
12 *Acad. Sci. U. S. A.* *101*, 15833 – 15839.
- 13 Seed, P.C., Passador, L., and Iglewski, B.H. (1995). Activation of the *Pseudomonas aeruginosa*
14 *lasI* gene by LasR and the *Pseudomonas* autoinducer PAI: an autoinduction regulatory hierarchy. *J.*
15 *Bacteriol.* *177*, 654 – 659.
- 16 Solano, C., Echeverez, M., and Lasa, I. (2014). Biofilm dispersion and quorum sensing. *Curr. Opin.*
17 *Microbiol.* *18*, 96 – 104.
- 18 Sousa, A., Bourgard, C., Wahl, L.M., and Gordo, I. (2013). Rates of transposition in *Escherichia*
19 *coli*. *Biol. Lett.* *9*, 20130838.
- 20 Stevens, A.M., and Greenberg, E.P. (1997). Quorum sensing in *Vibrio fischeri*: essential elements
21 for activation of the luminescence genes. *J. Bacteriol.* *179*, 557 – 562.
- 22 Tabor, J.J., Salis, H.M., Simpson, Z.B., Chevalier, A.A., Levskaya, A., Marcotte, E.M., Voigt,
23 C.A., and Ellington, A.D. (2009). A synthetic genetic edge detection program. *Cell* *137*, 1272 –
24 1281.
- 25 Tamsir, A., Tabor, J.J., and Voigt, C.A. (2011). Robust multicellular computing using genetically
26 encoded NOR gates and chemical *^*wires/’ . *Nature* *469*, 212 – 215.
- 27 Tan, C., Marguet, P., and You, L. (2009). Emergent bistability by a growth-modulating positive
28 feedback circuit. *Nat. Chem. Biol.* *5*, 842 – 848.
- 29 Winzer, K., Falconer, C., Garber, N.C., Diggle, S.P., Camara, M., and Williams, P. (2000). The
30 *Pseudomonas aeruginosa* lectins PA-IL and PA-III are controlled by quorum sensing and by
31 RpoS. *J. Bacteriol.* *182*, 6401 – 6411.
- 32 Wu, M., Su, R.-Q., Li, X., Ellis, T., Lai, Y.-C., and Wang, X. (2013). Engineering of regulated
33 stochastic cell fate determination. *Proc. Natl. Acad. Sci.* *110*, 10610 – 10615.
- 34 Xiong, W., and Ferrell, J.E. (2003). A positive-feedback-based bistable “memory module” that

governs a cell fate decision. Nature 426, 460 - 465.

Figure legends

Figure 1. QS crosstalk dissected using synthetic gene circuits. (A) LuxR can crosstalk with C12 to activate pLux. Top panel: schematic diagram of a synthetic gene circuit where a constitutive promoter (gray arrow) regulates LuxR (purple rectangle) expression. LuxR protein (purple bars), when dimerized and bound with C6 or C12, can activate pLux (purple arrow) to induce GFP (green rectangle) expression. The autoinducers, genes, and promoters are color coded so that naturally paired partners are in the same color. Bottom panel: dose response of the circuit when induced with C6 (gray) or C12 (black). (B) LasR can crosstalk with pLux when bound with C12. Top panel: schematic diagram of a circuit similar to that in (A), where a constitutive promoter regulates LasR (cyan rectangle) expression. LasR protein, when bound with C6 or C12, can activate pLux to induce GFP expression. Bottom panel: Dose response of this circuit when induced with C6 (gray) or C12 (black). Bar heights are averages of three independent flow cytometry measurements shown as mean \pm SD. (C) Summary of crosstalk induction of all 16 different combinations, including inductions by both chemicals and corresponding synthase genes. The four combinations shown in (A) and (B) are highlighted with a gray background. Quantified results for other combinations are included in Figure S1.

Figure 2. Signal crosstalk causes shrinkage of bistable region. (A) Schematic diagram of a synthetic gene circuit where the pLux promoter regulates expression of LuxR, which in turn can bind with C6 or C12 to further activate pLux, forming a positive feedback loop (shown as simplified diagram). GFP under the regulation of pLux serves as the readout for LuxR levels. All components are color coded similarly as in Figure 1. (B) The average of three replicate flow cytometry measurements is plotted as a square with error bars for each dose of C6 induction, where red indicates Initial ON cells while blue denotes Initial OFF cells. Solid lines represent results calculated from model fittings. The bistable region ranges from 0 to 10^{-9} M

1 C6. Labels 1 and 2 indicate representative experiments within the region to be shown as
2 histograms in (D). (C) Similar experiments as in (B) but with C12 inductions. The bistable
3 region ranges from 10^{-8} to 10^{-6} M C12. Labels 3 and 4 indicate representative experiments
4 within the bistable region to be shown as histograms in (D). (D) Histograms of flow
5 cytometry measurements labeled in (B) and (C). One representative measurement from each
6 point is shown. No bimodal distributions are observed.

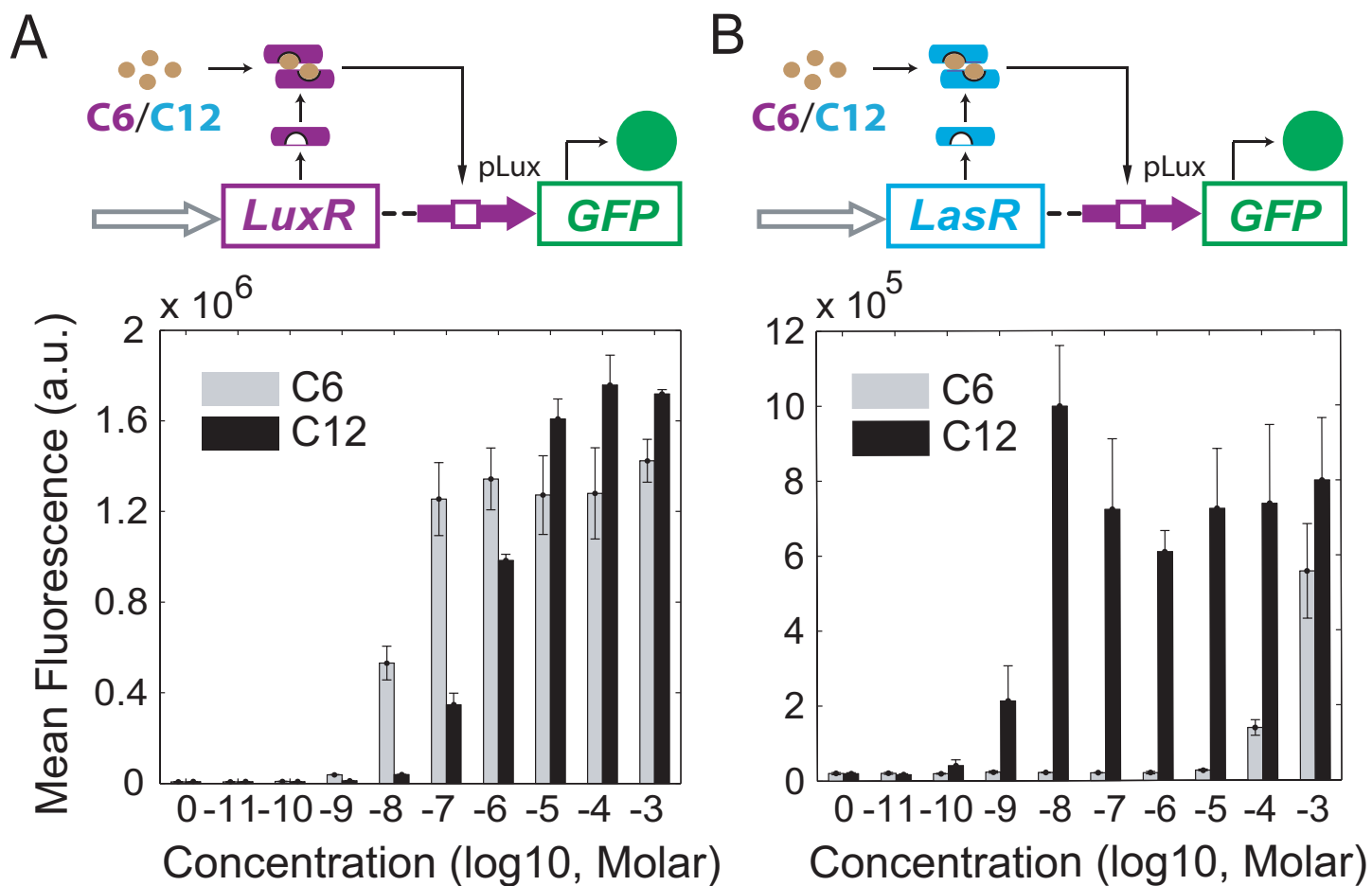
7
8 **Figure 3. Promoter crosstalk induces mutation and leads to population heterogeneity.** (A)

9 Schematic diagram of a synthetic LasR-pLux positive feedback circuit. GFP under the
10 regulation of pLux serves as the readout for LuxR levels. All components are color coded
11 similarly to Figure 1. (B) The average of three replicate flow cytometry measurements is
12 plotted as a square with error bars for each dose of C12 induction. Blue denotes Initial OFF
13 cells, while green and red indicate the Initial ON cells induced with 10^{-4} M C12 and 10^{-9} M
14 C12 before being re-diluted into concentrations of C12, respectively. Labels 1, 2, 3, and 4
15 indicate experiments to be shown in detail as histograms in (C). (C) Histograms of flow
16 cytometry measurements labeled in (B). One representative measurement from each point is
17 shown. A bimodal distribution is only observed for label 3: which is Initial ON cells (induced
18 with 10^{-9} M C12 before redilution) at 10^{-8} M C12. (D) DNA analysis for the Initial ON
19 samples shown as red in (B). Top: Plasmid DNA was extracted and digested with *EcoRI* and
20 *PstI*, and agarose gel electrophoresis results indicated gene mutation happened in samples
21 with 10^{-8} M and higher doses of C12. Lane 1 is the wild-type plasmid as the control, lanes 2 to
22 9 are samples in 10^{-11} to 10^{-4} M C12, and Lane 10 is the 1kb DNA marker. V: vector; F:
23 wild-type DNA fragment (the LasR-pLux positive feedback circuit); M: mutated fragment.
24 Bottom: Schematic representation of the mutation and the features of IS10 transposase
25 insertion: the target site (first CGCGTAGCG) in the LasR gene, its duplication (second
26 CGCGTAGCG) due to insertion of IS10 transposase, and the IS10 sequence (red box and
27 shown in *italics*).

28
29 **Figure 4. Model predictions and experimental validations of mutation induced**
30 **trimodality.** (A) Model predictions of GFP expression at several transposition rates: high (red,

1 $k_3=3.6e-6$), low (green, $k_3=4e-7$), and none (blue, $k_3=0$). Histograms were constructed from
 2 8000 single cell stochastic simulations at 1000 ($k_3=3.6e-6$) and 1900 ($k_3=0$ and $k_3=4e-7$)
 3 minutes. **(B)** Experimental validation of the model predictions in **(A)**. Red and green curves
 4 correspond to the high and low transposition rates from **(A)**, and they exhibit similar bi- and
 5 trimodal responses, respectively. No blue curve is included because mutation could not be
 6 eliminated entirely experimentally. **(C)** Representative stochastic simulations of single cell
 7 fluorescence starting from the ON state. All possible transitions are shown. Inset diagram
 8 illustrates all possible state transitions in the simulation. **(D)** Model predictions of GFP
 9 expression with low transposition rate showing temporal evolution of the population from
 10 primarily ON cells at an early time (green), to trimodal distributions at intermediate time
 11 (blue), eventually falling into a primarily Mutated state at late time (red). **(E)** Flow cytometry
 12 measurements taken at 12 hours (green), 24 hours (blue), and 32 hours (green). Populations
 13 show similar dynamics to those predicted by the model in **(D)**, starting with a large ON peak,
 14 transitioning to a trimodal distribution, then into primarily Mutated or OFF cells.

Figure 5. Fluorescence microscopy validation of mathematical model predictions. **(A)**
 17 GFP fluorescence (top) and phase contrast (bottom) images of cells growing in the
 18 microfluidic chamber at 0, 8, 16, and 24 hours. Magnification: 40x. **(B)** Normalized
 19 fluorescence expression of representative cells from **(A)**, showing similar behavior to that
 20 predicted by the model from Figure 4C. Four cells are colored corresponding to the scenarios
 21 in Figure 4C, and the other 11 cells are grey. Each trajectory follows one cell, with the
 22 trajectory branching as the cells divide. One frame equals five minutes. **(C)** Diagram of the
 23 mechanism for trimodality. Each “valley” represents one state. The blue curve represents the
 24 landscape at 37 °C, and the dotted grey curve is the landscape at 34 °C. At 37 °C, ON state
 25 cells can more easily transition to the Mutated state because of the low barrier; while at 34 °C,
 26 the barrier between ON and Mutated states increases, resulting in more ON cells transitioning
 27 to OFF state and promoting the emergence of trimodality.



C

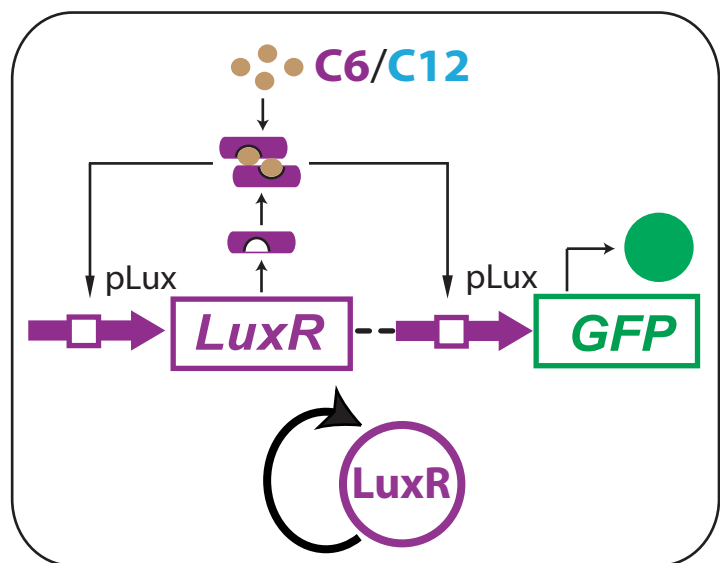
Summarization of the crosstalk between LuxR/I and LasR/I signal systems.

	LuxR- 3OC6HSL	LuxR- 3OC12HSL	LasR- 3OC6HSL	LasR- 3OC12HSL	LuxR- LuxI	LuxR- LasI	LasR- LuxI	LasR- LasI
pLux	+	+	-*	+	+	+	-	+
pLas	-	-	-*	+	-	-	-	+

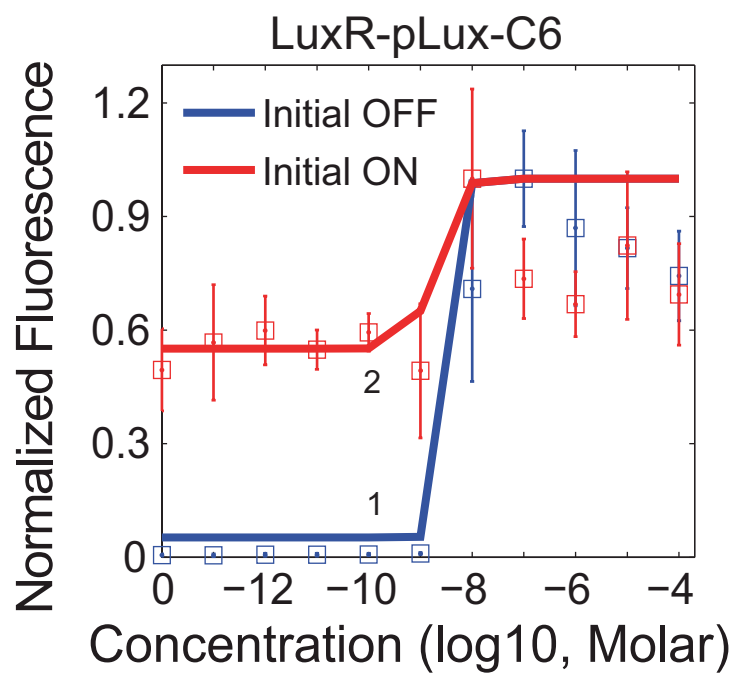
1: Black "+" indicates the original pairs; red "+" signifies pairs showing crosstalk.

2: "*" indicates LasR could only activate the promoter at high 3OC6HSL concentration.

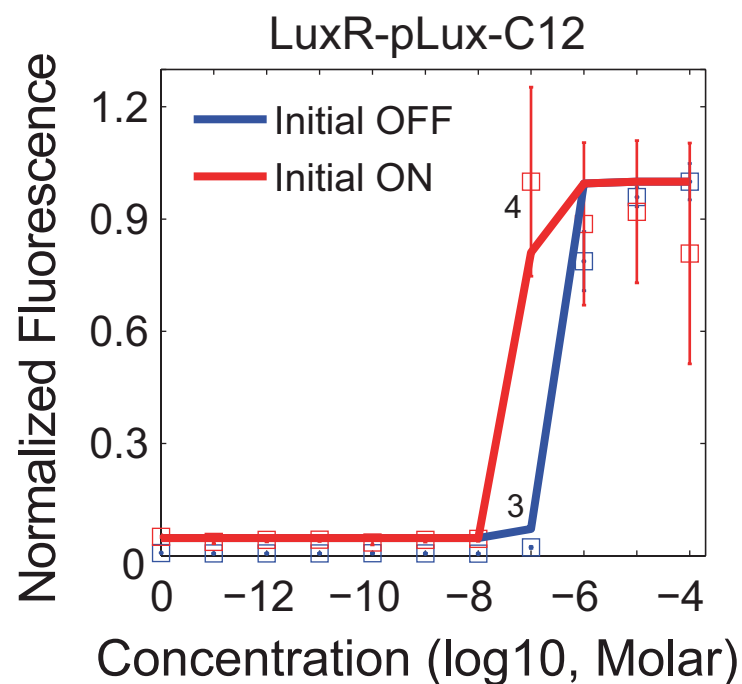
A



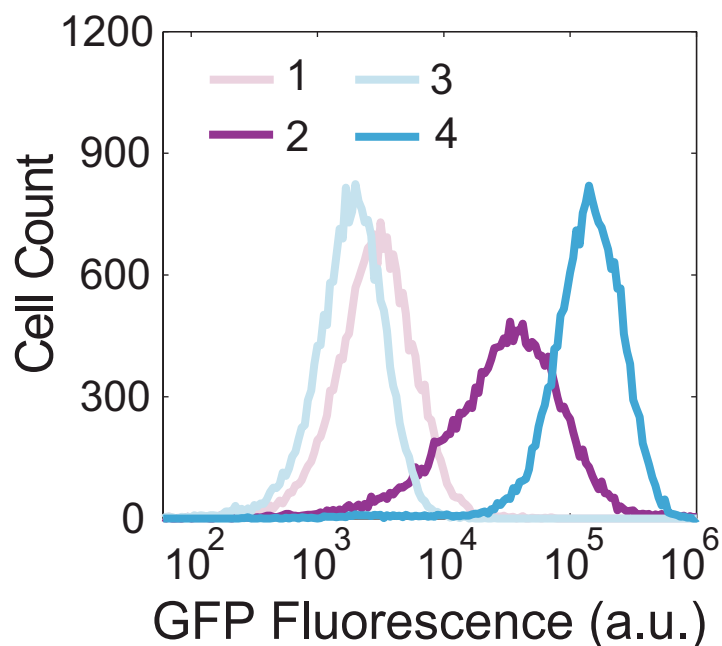
B



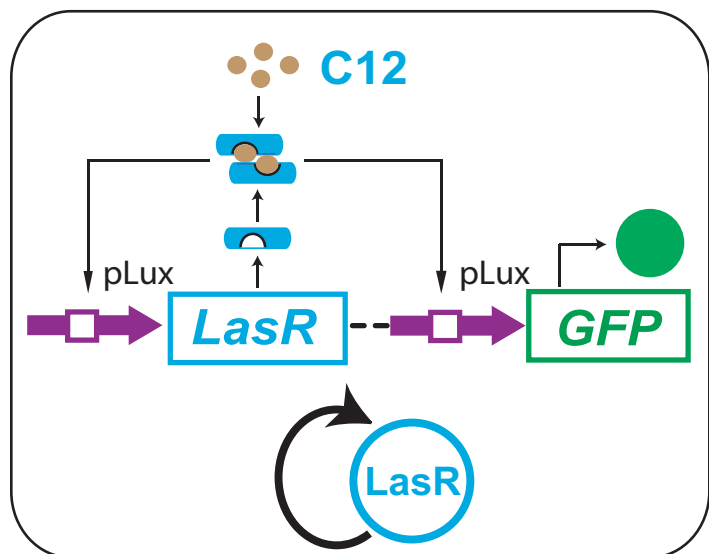
C



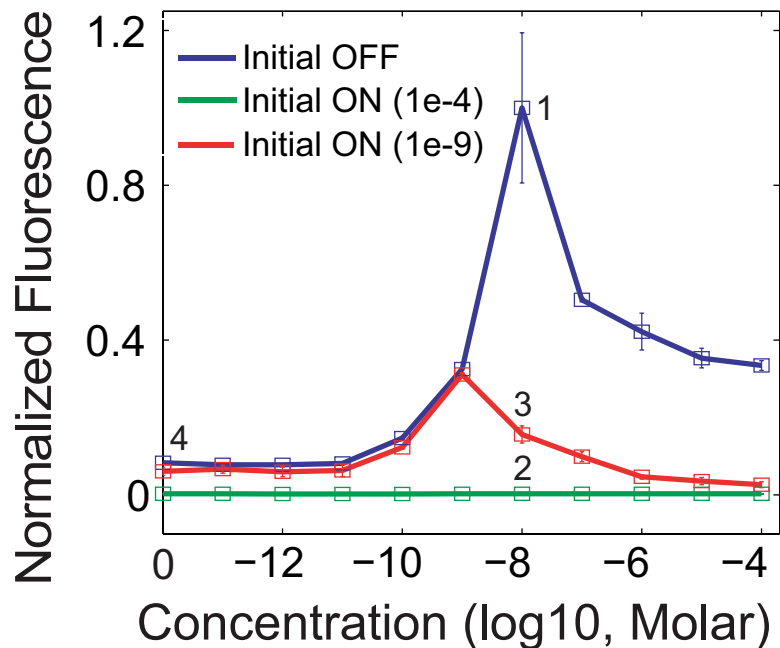
D



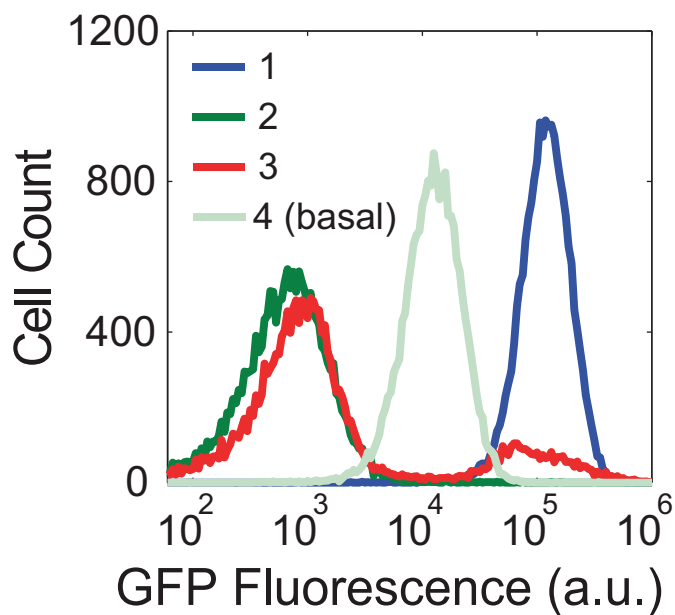
A



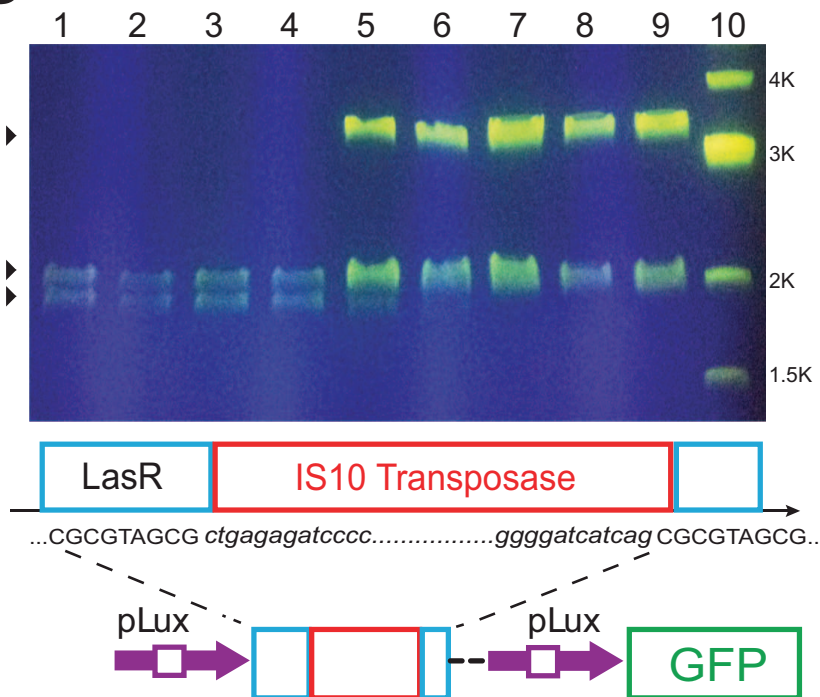
B



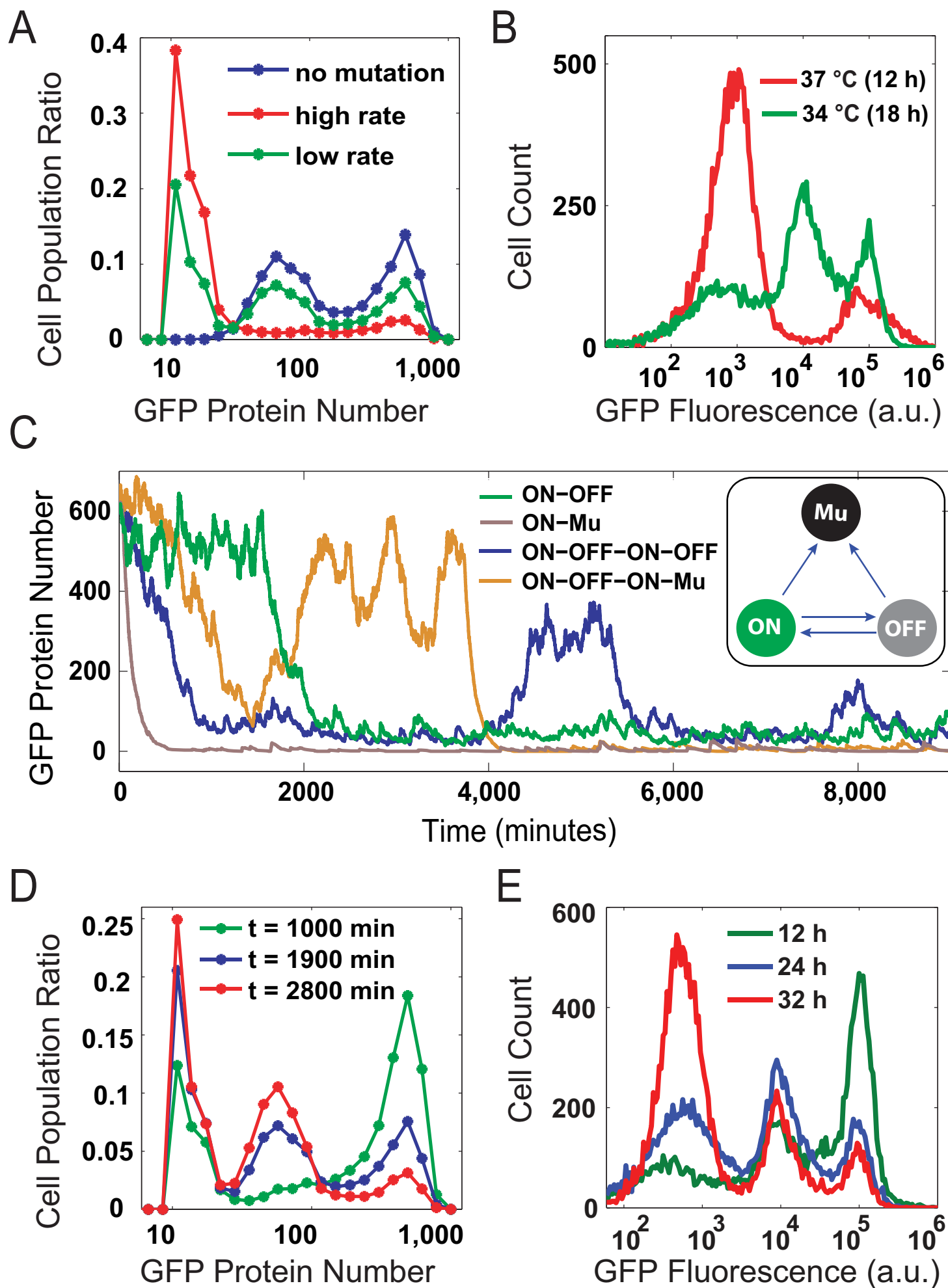
C



D



Figure



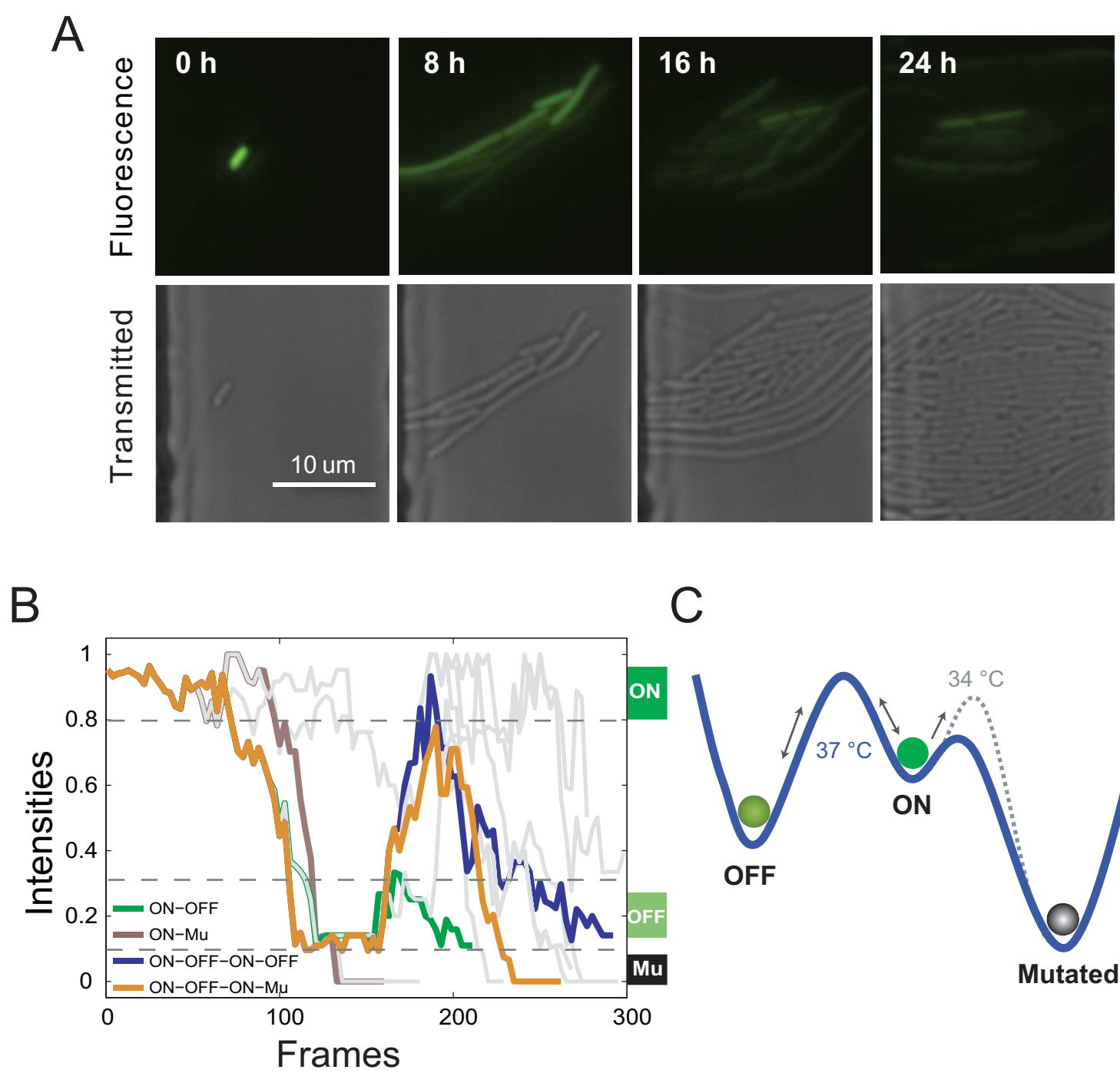


Figure S1

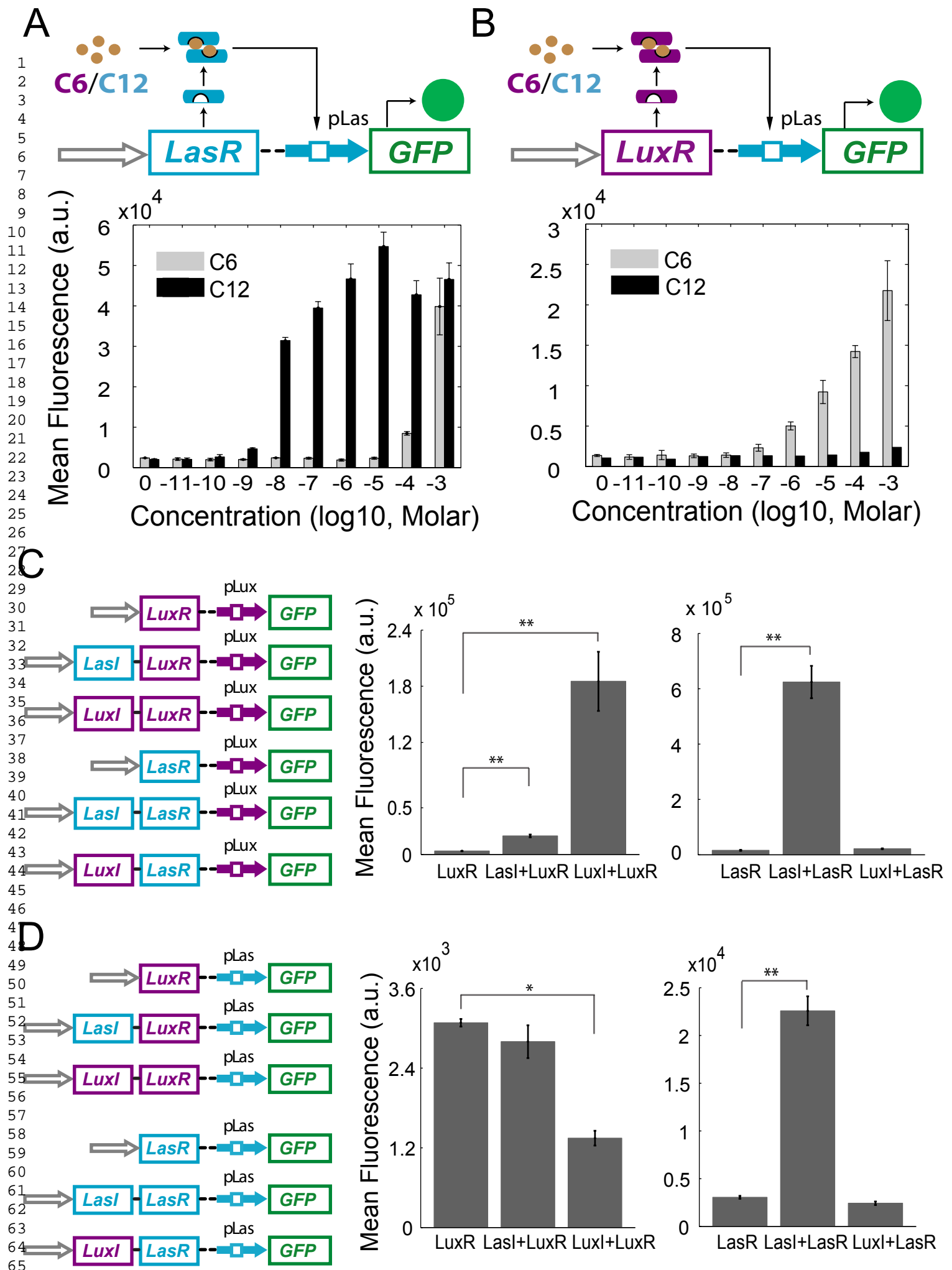
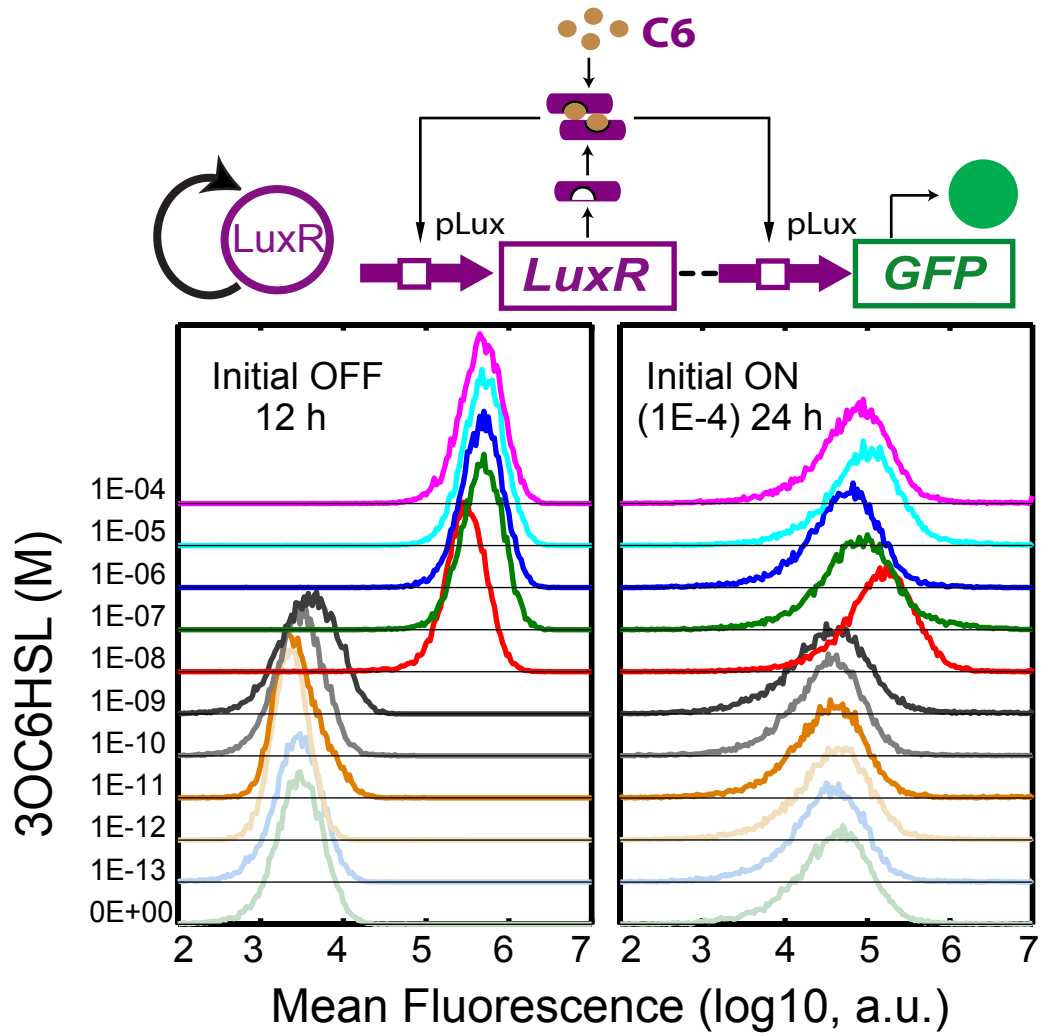


Figure S2

A



B

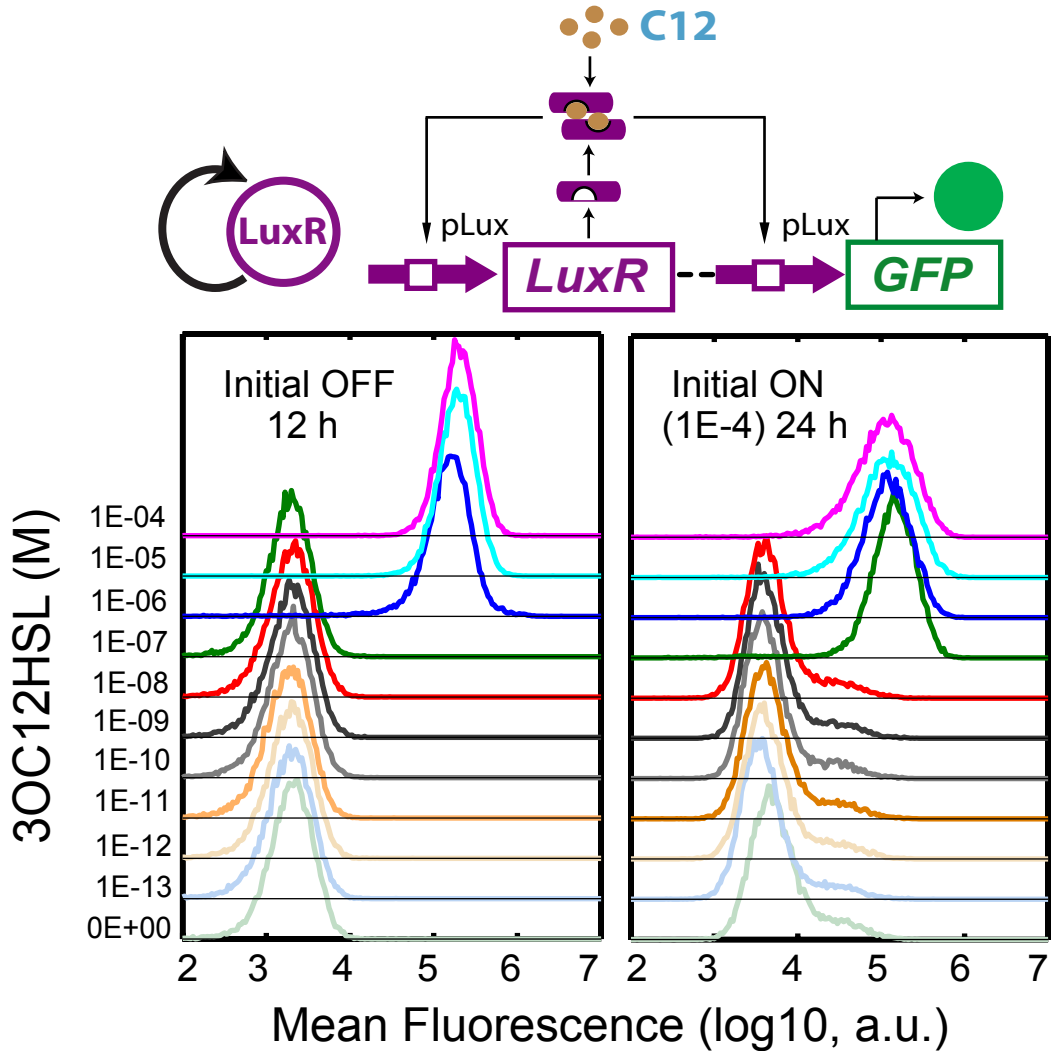


Figure S3

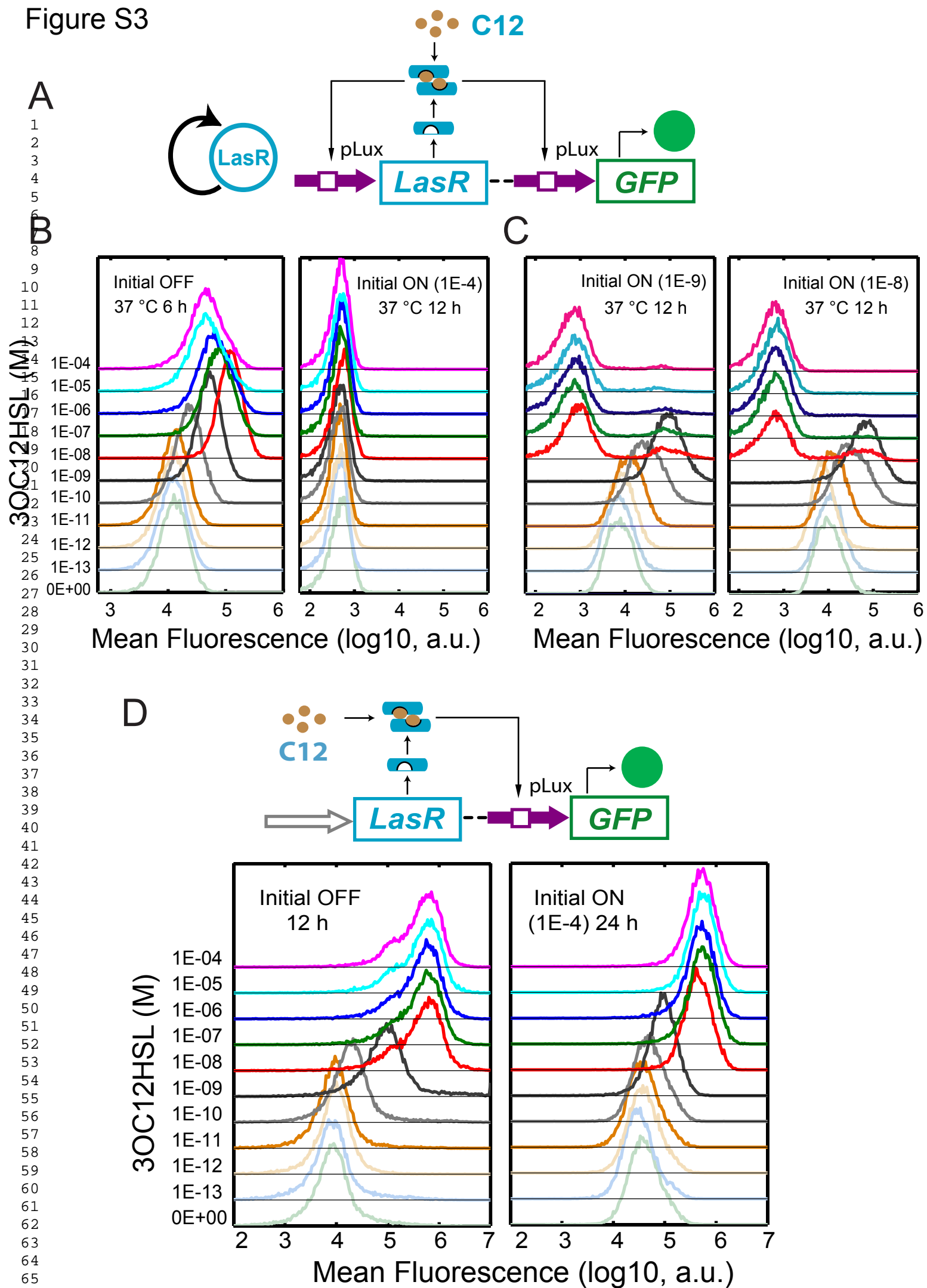
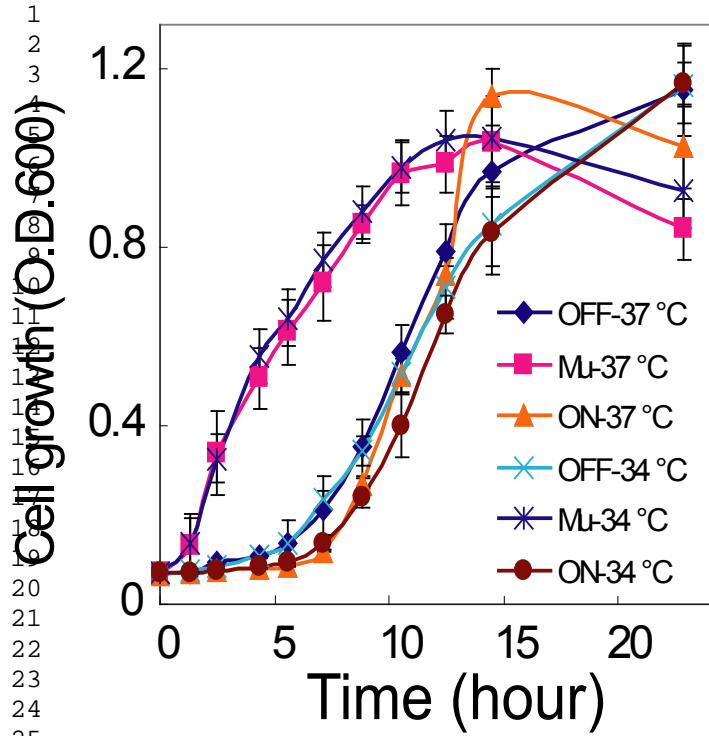
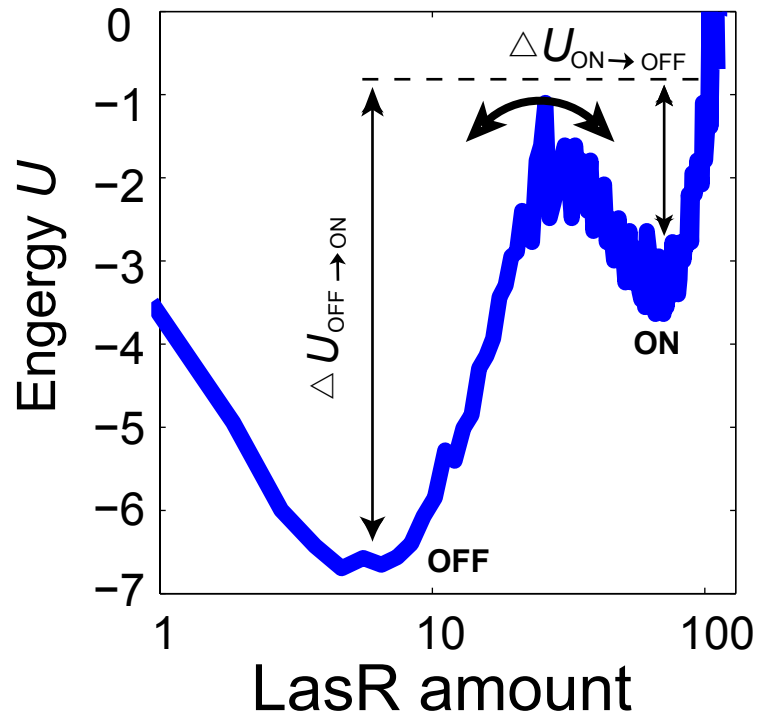


Figure S4

A



C



B

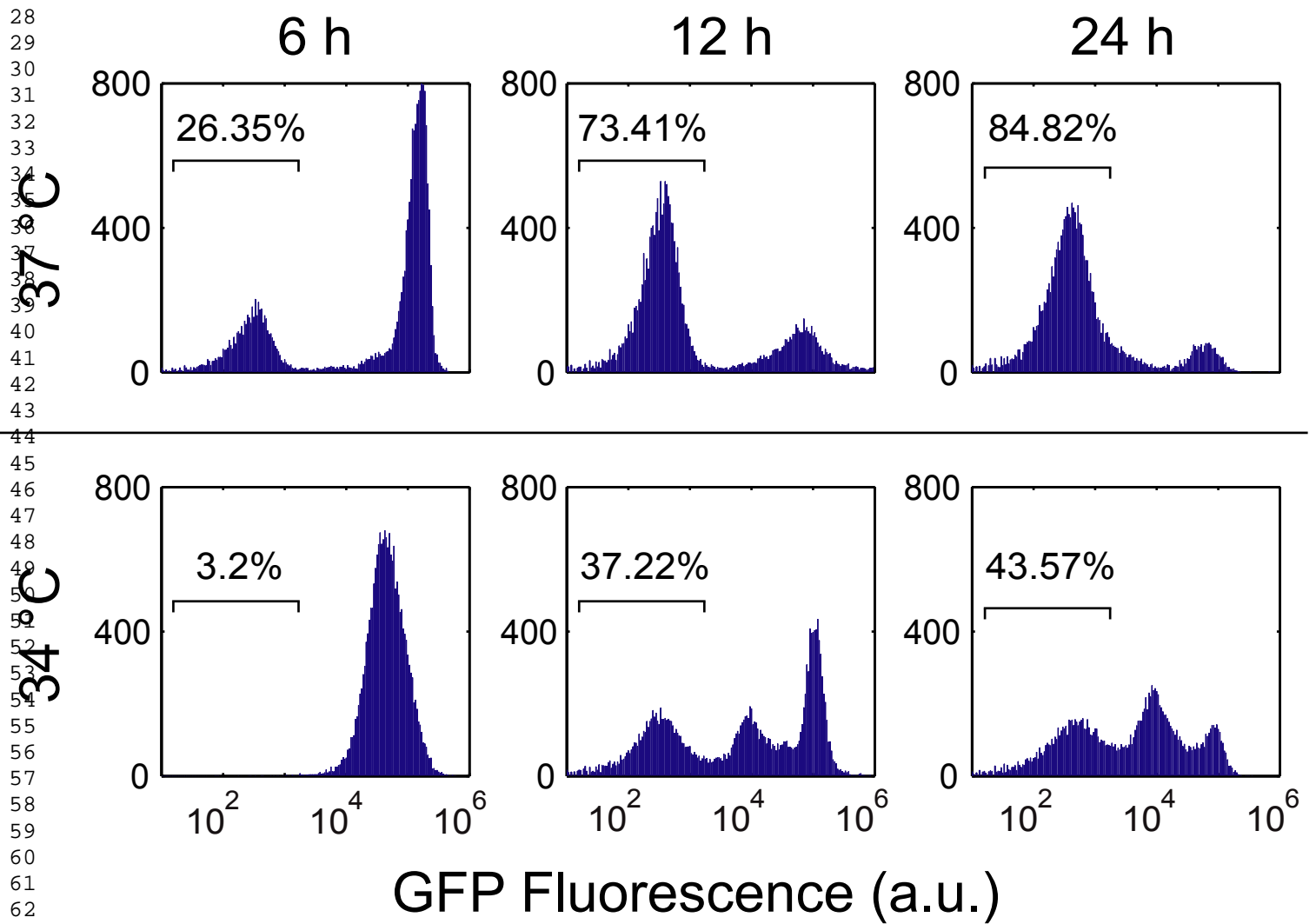
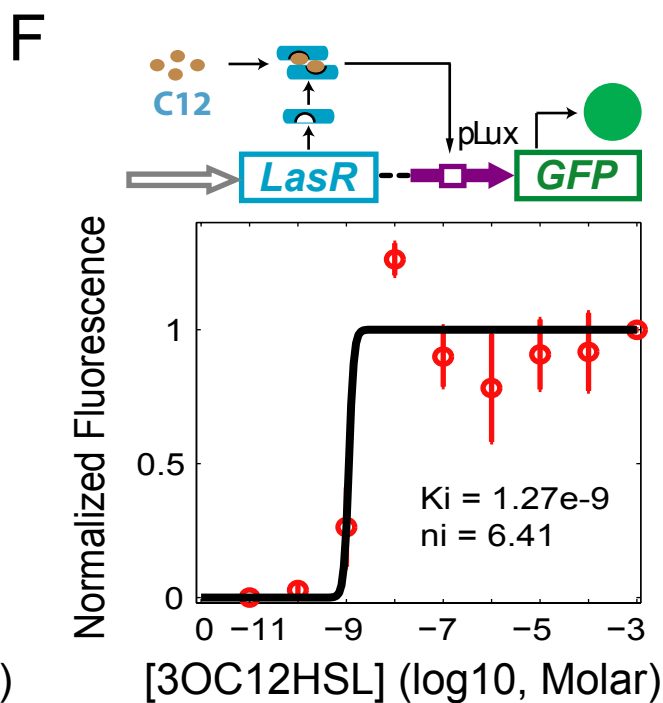
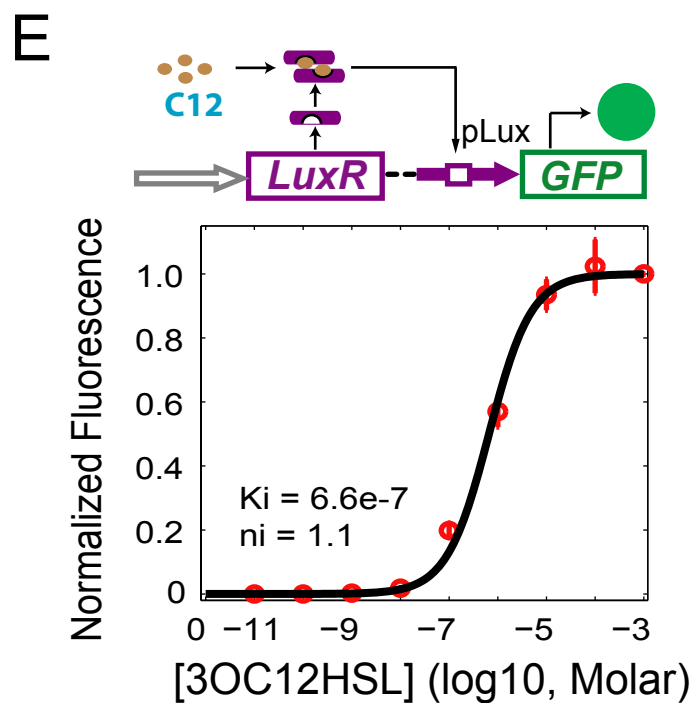
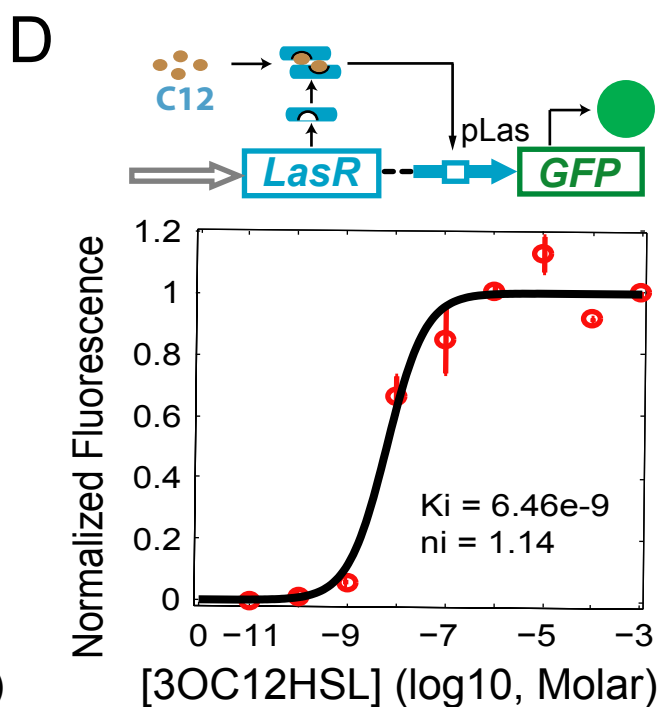
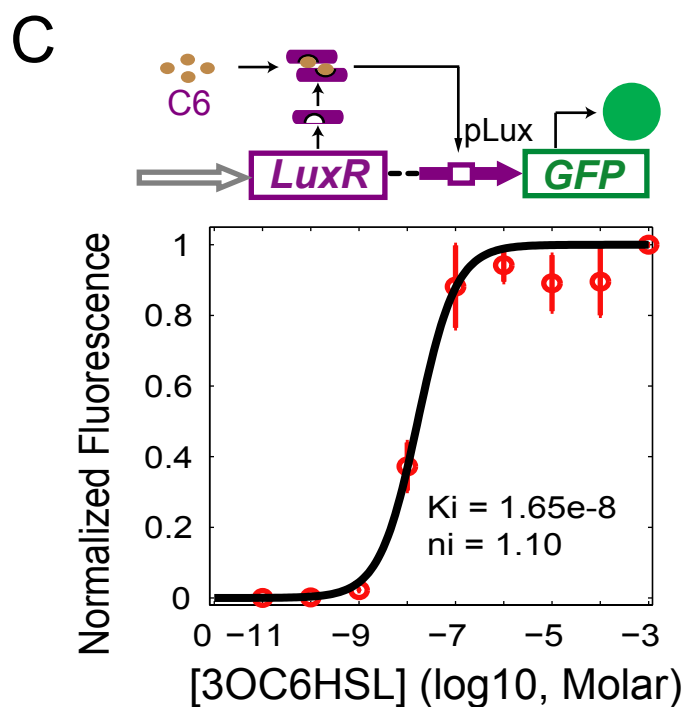
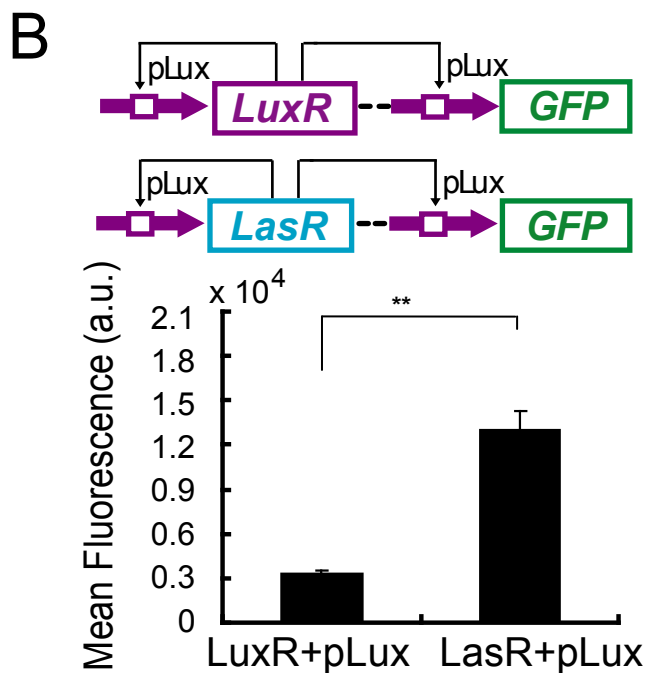
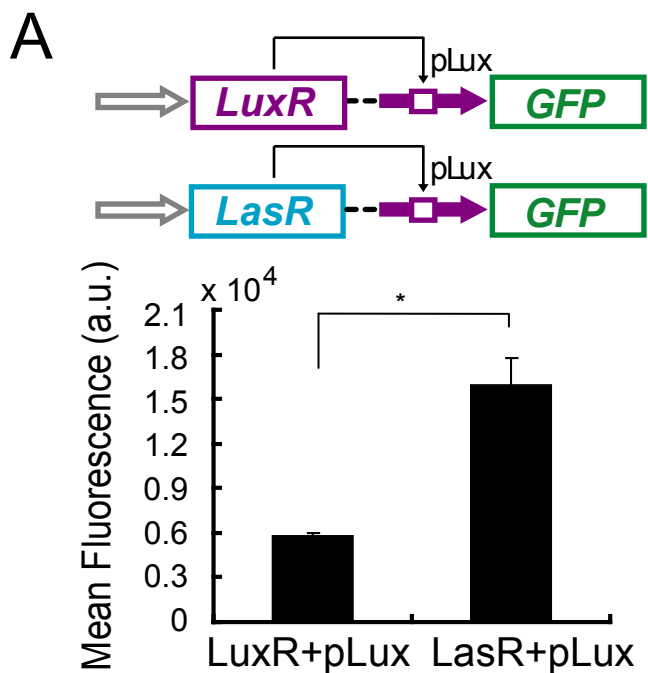


Figure S5

1
2
3
4
5
6
7
8
9
10
11
12
13
14
15
16
17
18
19
20
21
22
23
24
25
26
27
28
29
30
31
32
33
34
35
36
37
38
39
40
41
42
43
44
45
46
47
48
49
50
51
52
53
54
55
56
57
58
59
60
61
62
63
64
65



Supplemental Figure and Movie Legends:

Figure S1, related to Figure 1. QS crosstalk dissected using synthetic gene circuits. (A)

High concentrations of C6 can crosstalk with LasR-pLas. Top panel: schematic diagram of the synthetic gene circuit (CP-LasR-pLas). Bottom panel: dose response of the circuit when induced with C6 or C12. Compared to original pair of LasR-C12, the pLas promoter can only be activated by LasR with extremely high C6 concentration (signal crosstalk). **(B)** Promoter crosstalk of C6-LuxR with pLas is observed under high concentrations of autoinducer. Top panel: schematic diagram of the circuit (CP-LuxR-pLas). Bottom panel: Dose response of this circuit when induced with C6 or C12. LuxR can bind with C6 to activate pLas starting from 10^{-6} M (promoter crosstalk), while it cannot with C12. **(C)** Characterizing the crosstalk with the pLux promoter using synthase genes. LuxR, with either LuxI or with LasI, can activate pLux, while LasR with LasI can activate pLux. Left: schematic diagram of the synthetic gene circuits constructed to test crosstalk. LasI (cyan) and LuxI (purple) synthesize C12 and C6 molecules in cells, respectively. Right: GFP fluorescence in cells carrying the circuits was measured by flow cytometry at 12 h. LasI with LuxR, and LasI with LasR can significantly activate pLux (signal crosstalk, and promoter crosstalk, respectively). **(D)** Characterizing the crosstalk to the pLas promoter using synthase genes. No significant crosstalk was observed for LuxR- or LasR-pLas combinations. Left: schematic diagram of the synthetic gene circuits constructed. Right: GFP fluorescence in cells carrying the circuits was measured at 12 h. Both LasI-LuxR and LuxI-LuxR cannot activate pLas, and the latter shows ~ two-fold inhibition, and no signal crosstalk is observed for LasR-pLas. All the data are averages of three independent measurements shown as mean \pm SD (* p <0.05, and ** p <0.01).

Figure S2, related to Figure 2. Hysteresis of the LuxR-pLux positive feedback circuit. (A)

C6 induced hysteresis of the LuxR-pLux positive feedback circuit. Flow cytometry measurements of GFP expression for initial OFF cells (left) at 12 h and initial ON cells (right) at 24 h and 37 °C under different concentrations of C6 induction. Initial ON cells were collected from the cells induced with 10^{-4} M C6 for 6 hours and diluted twice into fresh media with the same concentrations of C6 at 12 h and 24 h. The positive feedback circuit displays

1 hysteresis with a bistable region from 0 to 10^{-8} M C6. No bimodal distribution was observed.
2
3 **(B)** C12 induced hysteresis of the LuxR-pLux positive feedback circuit. Flow cytometry
4 measurements of GFP expression for initial OFF cells (left) at 12 h and initial ON cells (right,
5 induced with 10^{-4} M C12 for 6 hours before redilution) at 24 h and 37 °C under C12 induction.
6 The initial ON cells were collected and diluted twice into new medium with the same
7 concentrations of C12 at 12 h and 24 h. The positive feedback circuit displays hysteresis with
8 a bistable region from 10^{-8} to 10^{-6} M C6. No bimodal distribution was observed.
9

10
11
12
13
14
15
16
17 **Figure S3, related to Figure 3. Hysteresis of the LasR-pLux circuits.** **(A)** Schematic
18 representation of the LasR-pLux positive feedback loop induced with C12. **(B)** Flow
19 cytometry measurements of GFP expression for initial OFF cells (left) at 6 h and initial ON
20 cells (right) at 12 h and 37 °C under different concentrations of C12 induction. For initial OFF
21 cells, GFP expression increases with C12 concentration, but begins to decrease uniformly
22 when C12 induction exceeds 10^{-8} M. For initial ON cells (induced with 10^{-4} M C12 before
23 redilution), all the samples exhibit unimodal minimal fluorescence signals that are even lower
24 than the basal GFP expression of initial OFF cells. **(C)** Initial OFF cells were first induced
25 with 10^{-9} or 10^{-8} M at 37 °C for 6 hours to become the new Initial ON cells, which were then
26 collected and rediluted into fresh media with different doses of C12. These two Initial ON
27 groups show a similar GFP expression pattern: unimodal distributions similar to the initial
28 OFF cells for samples in the lower inducer concentrations of 0 to 10^{-9} M, and bimodal
29 distributions within the higher concentration range of 10^{-8} to 10^{-4} M C12. GFP fluorescence
30 was measured by flow cytometry at 12 h. **(D)** C12 induced hysteresis of the CP-LasR-pLux
31 circuit. Flow cytometry measurements of GFP expression in initial OFF cells (left) at 12 h and
32 initial ON cells (right, induced with 10^{-4} M C12 for 6 hours before redilution) at 24 h and 37
33 °C under C12 induction. Results show that the initial OFF and ON cells show a similar
34 distribution pattern, and both exhibit unimodal expression without hysteresis.
35
36
37
38
39
40
41
42
43
44
45
46
47
48
49
50
51
52
53
54
55

56 **Figure S4, related to Figure 4.** **(A)** Growth curves for initial ON, OFF and Mutated cells in
57 10^{-8} M C12 at 37 °C and 34 °C. The initial ON and OFF cells' growth curves were similar,
58 with a long lag phase in 10^{-8} M C12, while the Mutated cells directly entered exponential
59
60
61
62
63
64
65

1 growth phase. All populations reached stationary phase after about 15 hours. The three cell
2 types show similar growth curves at 37 °C and 34 °C, indicating that growth temperature does
3 not significantly influence their growth rate. (B) Temperature changes the transposition rate.
4 Top: temporal evolution of the initial ON cells grown in 10⁻⁸ M C12 at 37 °C. Bottom: time
5 course of the same initial ON cells grown in 10⁻⁸ M C12 but at 34 °C. Flow cytometry was
6 used to measure the GFP fluorescence at 6 h, 12 h, and 24 h. For each measurement, the
7 percentage of Mutated state cells was calculated. Data shows that higher temperature
8 increases the transposition rate and IS10 transposase insertion, which promotes the transition
9 from the ON state to the Mutated state. (C) Quasi-potential U and the transition dynamics
10 between stable steady states in the LasR-pLux positive feedback system (without genetic
11 mutation). The lower ‘valley’ (with lower potential U) is the stable OFF state and the higher is
12 the stable ON state. According to the stochastic simulation, the energy barrier $\Delta U_{\text{OFF} \rightarrow \text{ON}}$ is
13 much greater than $\Delta U_{\text{ON} \rightarrow \text{OFF}}$, which suggests it is easier for ON state cells to transition to the
14 OFF state. The energy function is calculated according to the probability density distribution
15 of steady state LasR concentrations in each cell.

16
17
18
19
20
21
22
23
24
25
26
27
28
29
30
31
32
33 **Figure S5, related to Figures 2 and 4. Model parameter determination.** (A) Comparison
34 of the basal GFP expression from the pLux promoter between the two linear CP-LuxR-pLux
35 and CP-LasR-pLux circuits. (B) Comparison of basal GFP expression from the pLux
36 promoter between the two LuxR-pLux and LasR-pLux positive feedback circuits. All the data
37 shows that the leakage from the pLux promoter in LasR-pLux circuits is greater than in
38 LuxR-pLux circuits. All the data were averages of three independent measurements shown as
39 mean \pm SD (* p <0.05, and ** p <0.01). Parameters determination from experimental tests: (C)
40 the CP-LuxR-pLux circuit induced with C6; (D) the CP-LasR-pLas circuit induced with C12;
41 (E) the CP-LuxR-pLux circuit induced with C12; (F) the CP-LasR-pLux circuit induced with
42 C12. (C) and (D) are the original pairs used to test the functionality of all modules, while (E)
43 and (F) were used to characterize the signal and promoter crosstalk. All of the red data points
44 represent the mean of three independent measurements shown as mean \pm SD. The solid black
45 curves, corresponding Hill coefficients (ni), and dissociation constants (K_i) between
46 LuxR/LasR and C6/C12 were fitted from the dose response curves by the same fitting method
47
48
49
50
51
52
53
54
55
56
57
58
59
60
61
62
63
64
65

used in our previous work (Ellis et al., 2009; Wu et al., 2013).

Movie S1, related to Figure 5. A time lapse movie corresponding to Fig. 5A, for about 28 hours at 34 °C.

1
2
3
4
5
6
7
8
9
10
11
12
13
14
15
16
17
18
19
20
21
22
23
24
25
26
27
28
29
30
31
32
33
34
35
36
37
38
39
40
41
42
43
44
45
46
47
48
49
50
51
52
53
54
55
56
57
58
59
60
61
62
63
64
65

1
2
3
4
5
6
7
8
9
10
11
12
13
14
15
16
17
18
19
20
21
22
23
24
25
26
27
28
29
30
31
32
33
34
35
36
37
38
39
40
41
42
43
44
45
46
47
48
49

Table S1, related to Figure 1. Autoinducer information

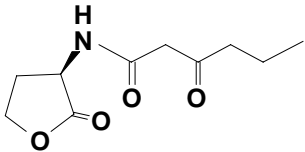
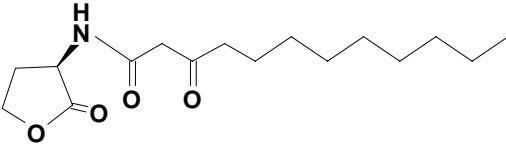
Full name	Molecular abbreviation	Molecular structure	Coding gene	Original binding regulator and promoter	Organism
N-(3-Oxohexanoyl)-L-homoserine lactone	3OC6HSL		LuxI (coding the enzyme, which synthesizes 3OC6HSL)	LuxR, pLux	<i>Aliivibrio fischeri</i>
N-(3-Oxododecanoyl)-L-homoserine lactone	3OC12HSL		LasI (coding the enzyme, which synthesizes 3OC12HSL)	LasR, pLas	<i>Pseudomonas aeruginosa</i>

Table S2, related to Figures 2 and 4. Parameters for the three positive feedback models

Parameters	Description	LuxR-pLux -3OC6HSL	LuxR-pLux -3OC12HSL	LasR-pLux -3OC12HSL	Source
k1	Transcription rate (min^{-1})	1.8	1.8	1.8	Ref.(Milo et al., 2010)
k2	Translation rate (min^{-1})	1.6	1.6	1.6	Ref.(Milo et al., 2010)
d1	LuxR/LasR degradation rate (min^{-1})	0.01	0.01	0.01	Ref.(Basu et al., 2005; Sayut and Sun, 2010)
d2	mRNA degradation rate (min^{-1})	0.33	0.33	0.33	Ref. (Bakshi et al., 2012; Milo et al., 2010)
c1	Leakage without LuxR or LasR protein (min^{-1})	0.08	0.08	0.08	Approximated according to Ref.(Danino et al., 2010)
c0	Leakage without AHL	0.007	0.007	0.03	Estimated and experiment indicated
Kd	Dissociation constant of LuxR-HSL dimerization	600	180	720	Estimated
Kn	Dissociation constant of [LuxR-HSL] ₂ binding DNA	2.6	14.7	177	Estimated
Ki	HSL concentration producing half occupation of pLux promoter	1.6e-8	6.6e-7	6.9e-9	Measured by experiments
ni	Hill coefficient	1.3	1.1	6.4	Measured by experiments

Table S3, related to Figure 4. Parameters for the genetic mutation event in the stochastic simulation of LasR-pLux positive feedback system

Parameters	Description	Value	Source
n	Cooperativity of IS10 transposase binding to the plasmid of LasR	5	Estimated and experiment indicated
K	Dissociation constant between transposase and the plasmid DNA	400	Estimated and experiment indicated
k3 (37 °C)	Transposition rate at 37 °C (min ⁻¹)	3.6e-6	Approximated according to experimental results and Ref.(Craig, 2002; Sousa et al., 2013)
k3 (34 °C)	Transposition rate at 34 °C (min ⁻¹)	4.0e-7	Approximated according to experimental results
c1	Transcription rate after gene mutation (min ⁻¹)	0.01	Estimated and experiment indicated
k1	Leakage without LasR protein after gene mutation (min ⁻¹)	0.005	Estimated and experiment indicated

1
2
3
4
5
6
7
8
9
10
11
12
13
14
15
16
17
18
19
20
21
22
23
24
25
26
27
28
29
30
31
32
33
34
35
36
37
38
39
40
41
42
43
44
45
46
47
48
49
50
51
52
53
54
55
56
57
58
59
60
61
62
63
64
65

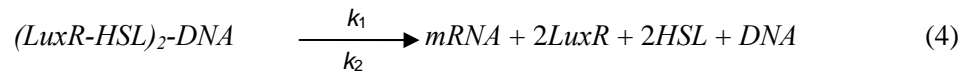
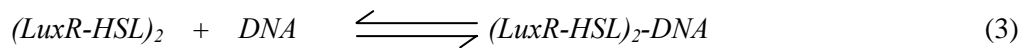
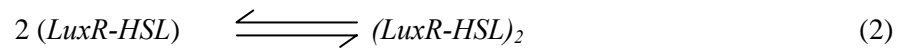
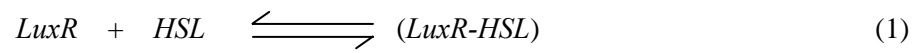
Table S4, related to Figure 1, 2, 3 and 4. Plasmids used in the circuits' construction. All materials are from the Registry of standard biological parts

Biobrick number	Abbreviation	Description
	in the paper	
BBa_R0062	pLux	Promoter activated by LuxR in concert with 3OC6HSL
BBa_R0079	pLas	Promoter activated by LasR in concert with 3OC12HSL
BBa_K176009	CP	Constitutive promoter family member J23107 actual sequence (pCon 0.36)
BBa_B0034	RBS	Ribosome binding site
BBa_B0015	T	Transcriptional terminator (double)
BBa_C0062	LuxR	LuxR repressor/activator
BBa_C0079	LasR	LasR activator
BBa_C0161	LuxI	Autoinducer synthetase for AI <i>from Aliivibrio fischeri</i>
BBa_C0178	LasI	Autoinducer synthetase for PAI from <i>Pseudomonas aeruginosa</i>
BBa_E0240	GFP	GFP generator
pSB1A3	pSB1A3	High copy BioBrick assembly plasmid

Supplemental Experimental Procedures:

Deterministic Model Construction

In the positive feedback loop circuit, LuxR production is controlled by the pLux promoter with only one LuxR-HSL binding site, which is bound and activated by the complex of LuxR and the autoinducer (3OC6HSL or 3OC12HSL, hereafter denoted as C6 and C12, respectively). GFP expression, as a reporter of the system, is regulated by the same pLux promoter and therefore follows the dynamics of LuxR. Therefore, we can directly analyze the LuxR dynamics in the model, comparing the output to the cells' fluorescence, without any loss of explanatory power. Since the LuxR-pLux and LasR-pLux positive feedback systems are characterized similarly and described by the same mathematical equations, we explain only the technical details for the LuxR-pLux positive feedback loop. Our model is based on the following biochemical reactions:



where *LuxR* is the monomer form of LuxR protein; *HSL* is the autoinducer 3OC6HSL; (*LuxR-HSL*) is the complex of LuxR bound with *HSL*; (*LuxR-HSL*)₂ is the dimer of (*LuxR-HSL*); (*LuxR-HSL*)₂-DNA represents (*LuxR-HSL*)₂ binding to the pLux promoter; *mRNA* is the messenger RNA of the LuxR gene; *k*₁ and *k*₂ are the transcription and translation rates, respectively; *d*₁ and *d*₂ are the degradation rates of mRNA and LuxR, respectively.

After C6 concentration reaches a certain threshold, LuxR binds to HSL molecules and forms the active LuxR monomers in the form of (*LuxR-HSL*) (Reaction 1). To quantitatively capture the relationship between the autoinducer concentration and the active LuxR

1 monomers, a Hill function is employed to represent the fraction of LuxR monomers bound by
 2 HSL (f):
 3

$$4 \quad f = [\text{HSL}]^{n_i} / ([\text{HSL}]^{n_i} + K_i^{n_i}) \quad [\text{Eq1}]$$

6 where n_i is the binding cooperativity (Hill coefficient) between LuxR and HSL, and K_i
 7 represents the dissociation constant between LuxR and HSL (the HSL concentration
 8 producing half conversion of LuxR monomers into *LuxR-HSL* complexes). It should be noted
 9 that different autoinducers will have different K_i values. Here we assume that the activator
 10 LuxR is abundant, and the fraction of active LuxR is independent from LuxR abundance in
 11 the cell.
 12

13 LuxR needs to form a dimer to bind the promoter and activate transcription. We describe
 14 the relationship between the dimer and the monomer as the following expression:
 15

$$16 \quad [\text{LuxR}_2] = [\text{LuxR}]^2 / K_d \quad [\text{Eq2}]$$

17 where K_d is the dissociation constant for LuxR dimerization. According to reaction (2), two
 18 (*LuxR-HSL*) molecules bind together to form a dimer and activate transcription. Additionally,
 19 it is necessary to point out that even without autoinducer *LuxR*₂ can still bind the pLux
 20 promoter and initiate leaky transcription of downstream genes. Taken together, the
 21 concentration of the functional LuxR dimer that will bind to pLux and activate its
 22 transcription is:
 23

$$24 \quad C = (c_0 + f^2) * [\text{LuxR}]^2 / K_d \quad [\text{Eq3}]$$

25 Here C represents the concentration of functional LuxR dimer (*(LuxR-HSL)*₂ and *LuxR*₂); c_0 is
 26 the fraction of *LuxR*₂ that can recognize and bind pLux in the absence of autoinducers; K_d is
 27 the dissociation constant for dimerization.
 28

29 (*LuxR-HSL*)₂ then recognizes and binds to the pLux promoter to form the
 30 (*LuxR-HSL*)₂-DNA complex together with RNA polymerase and other transcription factors to
 31 initiate transcription and produce mRNA (Reactions 3 and 4). So the expression of mRNA can
 32 be modeled as:
 33

$$34 \quad S_m = c_l + k_l C / (C + K_n) \quad [\text{Eq4}]$$

35 where S_m represents the production of mRNA; c_l represents the basal mRNA expression
 36
 37
 38
 39
 40
 41
 42
 43
 44
 45
 46
 47
 48
 49
 50
 51
 52
 53
 54
 55
 56
 57
 58
 59
 60
 61
 62
 63
 64
 65

without LuxR protein; k_l is the transcription rate; K_n is the dissociation constant between C and pLux promoter.

After transcription, mRNA is translated into LuxR protein (Reaction 5). Here we simplify the whole translation process and capture the production of LuxR protein in the form of:

$$S_p = k_2 * [\text{mRNA}] \quad [\text{Eq5}]$$

where S_p represents the synthesis of LuxR and k_2 is the translation rate.

Next, we take the constitutive degradation of mRNA in the cell into account (Reaction 6) with the equation:

$$D_m = d_1 * [\text{mRNA}] \quad [\text{Eq6}]$$

where d_1 is the degradation rate of mRNA.

Similarly, the degradation of LuxR protein (Reaction 7) is:

$$D_p = d_2 * [\text{LuxR}] \quad [\text{Eq7}]$$

where d_2 is the degradation rate of LuxR.

Finally, we combine the synthesis and degradation (Eq4, 5, 6, and 7) to find the rates of change of the concentrations of mRNA and LuxR:

$$\begin{cases} d[M]/dt = S_m - D_m \\ d[R]/dt = S_p - D_p \end{cases} \quad [\text{Eq8}]$$

where M and R represents mRNA of LuxR and LuxR monomers, respectively. Combining all the parameters, the two ODE equations can be rewritten as follows:

$$\begin{cases} \frac{d[M]}{dt} = c_1 + \frac{k_1 C}{C + K_n} - d_1 [M]; \\ \frac{d[R]}{dt} = k_2 [M] - d_2 [R]. \end{cases} \quad \text{Where} \quad \begin{cases} C = \frac{(c_0 + f^2) \cdot [R]^2}{K_d} \\ f = \frac{[\text{HSL}]^{n_i}}{[\text{HSL}]^{n_i} + K_i^{n_i}} \end{cases} \quad [\text{Eq9}]$$

These two ordinary differential equations were used to model the three positive feedback loops: LuxR-pLux-C6, LuxR-pLux-C12, and LasR-pLux-C12. Owing to the signal and promoter crosstalk, the dissociation constants K_i , K_d , and K_n may be different, as may also be the case with the Hill coefficients and leaky expression without autoinducer. Setting of parameter values is introduced below.

Stochastic Simulation Coupled with Genetic Mutation

The Gillespie algorithm was employed to perform stochastic simulations of the positive feedback loops (Gillespie, 1977). According to our deterministic model (Eq9), two equations capture the time evolution of the biochemical reactions. In this model, there are four independent events in total – mRNA production, mRNA decay, LuxR production, and LuxR decay – which are translated directly to the stochastic model. Simulation data was collected for 8000 cells, and each simulation was run for 40000 steps.

The energy-like function $U(x)$, which denotes the probability and direction of transitions between attractors in a noisy environment, can also be used to interpret state transitions (Zhou et al., 2012). After finishing all simulations, we first calculated the amount of LasR present in each cell (assuming the cells had reached steady state), then divided by the total number of cells. This yielded a probability density distribution of steady state LasR concentrations, which was used to calculate the energy function $U(LasR)$ by the following approach (Zhou et al., 2012):

$$U(LasR, t) \sim -\ln(P(LasR), t) \quad [\text{Eq10}]$$

where $P(LasR, t)$ is the steady-state probability for each LasR concentration at a given time t . In practice, the $P(LasR, t)$ was derived from the following equation:

$$P(LasR) = \text{hist}(LasR)/\text{Cellnum} \quad [\text{Eq11}]$$

where $\text{hist}(LasR)$ is a histogram of the amount of LasR in each cell and Cellnum is the total number of simulated cells. The energy-like function U gave us a more vivid and direct understanding of the quasi-potential landscape and the transition dynamics between stable steady states in this positive feedback system. The transition rates between ON and OFF states are decided by the energy barrier ΔU (Figure S4C). Unlike the typical bimodality emerged from bistable systems, C12-LasR-pLux positive feedback loop displayed an asymmetric bimodal distribution at a population level, which only happened from ON state to OFF state. The model suggests that this asymmetry comes from the different energy barrier of switching between ON and OFF states (Figure S4C).

To take the genetic mutation in the LasR-pLux positive feedback circuit into account, we

1 added another event in addition to mRNA and LasR production and degradation. Since the
2 genetic mutation only happened in initial ON cells, and because it is easier for cells in high
3 C12 concentration to mutate, we inferred that more LasR in the cell resulted in a higher
4 mutation probability. Moreover, the mutation occurred in the LasR open reading frame, so
5 theoretically the mutation probability is positive as long as the LasR gene is present. Here, we
6 used a Hill function to describe the probability of mutation:
7
8
9

$$Pm = [LasR]^n / (K^n + [LasR]^n) \quad [Eq11]$$

10 where Pm represents the probability of mutation; n is the Hill coefficient indicating the
11 cooperativity of mutation causing factors related to LasR concentration; and K represents the
12 dissociation constant in the complicated biochemical reactions. In the Gillespie simulation,
13 the mutation event, independent of the other four events, was described mathematically as:
14
15
16
17
18
19
20
21
22

$$Mu = k_3 * Pm * [LasR] \quad [Eq12]$$

23 where k_3 is the transposition rate; $[LasR]$ is the amount of LasR in the cell at a given time, and
24 Pm is the probability of mutation as described above. Generally, once the mutation has
25 happened, the LasR gene is broken into two parts and the functional mRNA of LasR cannot
26 be produced any more. Mutated cells theoretically retain the ability to switch state. However,
27 the probability of this occurring is small. In practice, for each cell, when the mutation event
28 had occurred, the transcription rate (k_l) and leaky expression from pLux (c_l) were reduced to
29 very low values, the cell would remain mutated, and the simulation was ended. By tuning the
30 transposition rate, we fit the parameters according to experimental data, which we then used
31 to make predictions.
32
33
34
35
36
37
38
39
40
41
42
43
44
45
46

47 Next, since the ON, OFF, and Mutation cells have different growth curves under the same
48 experimental conditions, growth rate differences between the three populations were added
49 into the model. From the growth curves, it can be seen that the initial ON and OFF cells'
50 growth curves were similar, with a long lag phase in 1e-8 M C12, while the Mutation cells
51 directly entered exponential growth. All three populations went to stationary phase after about
52 15 hours (Figure S4A). Instead of using a population balance model, we employed a simple
53 and efficient method to combine the stochastic model with population dynamics. The cells
54
55
56
57
58
59
60
61
62
63
64
65

1 with greater growth rate would acquire an extra advantage in their final quantity: each of the
2 three original populations was multiplied by its relative growth rate and then its ratio in the
3 three populations was adjusted.
4
5

6 To simplify the case, we chose three time points (2.5 h, 7.1 h and 12.5 h) and compared
7 their O.D. values (by $OD^{\text{Mutation}}/OD^{\text{ON}}$, $OD^{\text{OFF}}/OD^{\text{ON}}$, and $OD^{\text{ON}}/OD^{\text{ON}}$: ON cells grew slowest)
8 and then made an average to get an averaged relative growth rate, which then was taken into
9 the simulation results. So the final amount of Mutation cells (Fmu), OFF cells ($Foff$) and ON
10 cells (Fon) are:
11
12
13
14
15

$$16 \quad Fmu = Smu * (OD^{\text{Mutation}}/OD^{\text{ON}});$$

$$17 \quad Foff = Soff * (OD^{\text{OFF}}/OD^{\text{ON}});$$

$$18 \quad Fon = Son * 1;$$

19 where Smu , $Soff$, and Son are the primary number of cells which finished the simulation in the
20 Mutation, OFF, and ON states, respectively. Therefore, the proportions of Mutation cells
21 (Pmu), OFF cells ($Poff$), and ON cells (Pon) are:
22
23
24
25
26
27
28

$$29 \quad Pmu = Fmu/(Fmu + Foff + Fon);$$

$$30 \quad Poff = Foff/(Fmu + Foff + Fon);$$

$$31 \quad Pon = Fon/(Fmu + Foff + Fon);$$

32 In this way, the population with a greater growth rate acquired an advantage in its quantity
33 under identical conditions.
34
35
36
37
38
39
40
41

42 **Determinations of parameter values**

43 In the *E.coli* cells, even though the transformed plasmid is high-copy, there is also a
44 maximum expression value. According to the B10NUMB3R5 database(Milo et al., 2010),
45 each protein generally has no more than 1000 copies. Therefore, we chose 1000 molecules per
46 cell to be the maximum expression value of LuxR and LasR. All other parameters were
47 adjusted under this assumption.
48
49
50
51
52
53

54 Specifically, the transcription rate (k_1), translation rate (k_2), and degradation rates of mRNA
55 and LuxR (d_1 and d_2 , respectively) were estimated from previous reports and the
56 B10NUMB3R5 database (Table S2). Since pLux was the only promoter used in the positive
57 feedback circuits, the leaky expression without LuxR or LasR (c_1) did not change between
58
59
60
61
62
63
64
65

1 simulations, and it was estimated to be 0.08 min^{-1} . In addition, according to experimental
2 results, basal GFP expression in the absence of autoinducers (c_0) in the LasR-pLux positive
3 feedback circuit is about three times larger than in its LuxR-pLux counterpart (Figure S5A
4 and S5B). Therefore c_0 was set to 0.03 and 0.007 for LasR-pLux and LuxR-pLux, respectively.
5
6 The Hill coefficients (ni) and dissociation constants (K_i) between LuxR/LasR and the C6/C12
7 were fitted from the dose response curves (Figure S5C-S5F) by the same fitting method used
8 in our previous work (Ellis et al., 2009; Wu et al., 2013). Considering experimental variations,
9 parameters were adjusted within 10% relative error.

10
11 The generic parameters K_d and K_n are constant and fit to make the model consistent with
12 with experimental results (Figure 2B and 2C). With these fitted parameters, our model
13 captured the experimental hysteresis results and provided insights to understand the difference
14 between the three positive feedback loop variants induced by QS crosstalk. For example, K_d
15 in LuxR-pLux-C12 positive feedback was smaller than in LuxR-pLux-C6, while K_n was
16 larger for LuxR-pLux-C12. This suggests that C12 might bind more easily to LuxR (relative
17 to C6), but the original LuxR-C6 pair has higher affinity for the pLux promoter. Additionally,
18 K_n in the LasR-pLux positive feedback loop is much bigger for LasR-C12 than for either
19 LuxR-C6 or LuxR-C12, which indicates that the LasR-C12 dimer has less affinity for pLux,
20 and therefore it is more difficult for the system to reach saturation. The parameter
21 combination for the LasR-pLux positive feedback loop was used in the stochastic simulation
22 and for predicting trimodality.

23
24 To fit the probability of the LasR gene's mutation against experimental results at 37°C , we
25 first approximated the Hill coefficient (n) and the dissociation constant (K) based on the
26 difference between fluorescence values at the ON and OFF states. Different n and K
27 combinations were generated, and it was discovered that $n = 5$ and $K = 400$ best fit the
28 experimental data (Figure 4A and 4B). In addition, previous reports indicated that
29 transposition rates of IS elements in *E.coli* usually range from $1\text{e-}3$ to $1\text{e-}7 \text{ min}^{-1}$ (Craig, 2002;
30 Sousa et al., 2013). So the transposition rate in our model was estimated ($k_3 = 3.6\text{e-}6 \text{ min}^{-1}$)
31 according to the final experimental data (Figure 4B). To predict the trimodal response, k_3 was
32 adjusted but all the other parameters were held constant. With $k_3 = 4.0\text{e-}7 \text{ min}^{-1}$, the
33
34
35
36
37
38
39
40
41
42
43
44
45
46
47
48
49
50
51
52
53
54
55
56
57
58
59
60
61
62
63
64
65

1 simulation exhibited trimodality, which was validated by the experimental results at 34 °C
2
3 (Figure 4D and 4E).

4 All the parameter values are listed in Table S2 and S3.
5
6
7
8

9 **Mutation verification by DNA sequencing**

10 For the initial ON cells growing in 10^{-10} to 10^{-4} M C12, plasmids were extracted,
11 digested for genotyping, and sequenced. Several primers were used to check for
12 mutation. Following the order of assembly shown in Supplementary Fig. 16b, these
13 primers were: BB-N-Forward, LasR-C-Forward, GFP-N-Reverse, BB-C-Reverse, and
14 GFP-C-Forward. Descriptions and sequencing results for each primer are below.
15 Combining these results, we concluded that the mutation happened within the LasR
16 gene, and the other fragments and backbone were correct.
17
18
19
20

21 For convenience, all fragments are highlighted: pLux promoter: yellow; ribosomal
22 binding site: blue; LasR: cyan; IS10 transposase: pink; Terminator: red; GFP
23 generator: green; pSB1A3 vector: grey.
24
25
26
27

28 **BB-N-Forward**

29 Sequence: TGCCACCTGACGTCTAAGAA

30 Description: Forward, starting from the N terminal of the multiple cloning site (MCS)
31
32
33

34 Sequencing with BB-N-Forward on the vector verified the promoter pLux (yellow),
35 the ribosomal binding site (blue), part of LasR (cyan, 681 bp), and a new inserted
36 sequence (pink). This new sequence was determined to be part of an IS10
37 transposase gene according to BLASTn results from NCBI. The transposon target site
38 is also marked (Bold black, highlighted pink). Sequencing results are as follows:
39
40
41

42 >LasR-pLux-PF-BBF 1360 ABI

43 1→

```
44 CACGGAACTTAACCTATACAAATAGGCGTATCACGAGGCAGAATTTTCAGA  
45 TAAAAAAAAATCCTTAGCTTTTCGCTAAGGATGATTTCTGGAATTCGCGGCC  
46 GCTTCTAGAGACCTGTAGGATCGTACAGGTTTACGCAAGAAAATGGTTTG  
47 TTATAGTCGAATAAA TACTAGAGAAAGAGGAGAAA TACTAGATGGCCTTG  
48 GTTGACGGTTTTCTTGAGCTGGAACGCTCAAGTGGAAAATGGAGTGGAG  
49 CGCCATCCTCCAGAAGATGGCGAGCGACCTTGGATTCTCGAAGATCCTGT  
50 TCGGCCTGTTGCCTAAGGACAGCCAGGACTACGAGAACGCCTTCATCGTC  
51 GGCAACTACCCGGCCGCTGGCGGAGCATTACGACCGGGCTGGCTACGC  
52 GCGGGTCGACCCGACGGTCACTGTACCCAGAGCGTACTGCCGATTT  
53 TCTGGGAACCGTCCATCTACCAGACGCGAAAGCAGCACGAGTTCTTCGAG  
54 GAAGCCTCGGCCCGGCCTGGTGTATGGGCTGACCATGCCGCTGCATGG  
55 TGCTCGCGGCGAACTCGGCGCGCTGAGCCTCAGCGTGGAAAGCGGAAAACC
```

61
62
63
64
65

1
2
3
4
5
6
7
8
9
10
11
12
13
14
15
16
17
18
19
20
21
22
23
24
25
26
27
28
29
30
31
32
33
34
35
36
37
38
39
40
41
42
43
44
45
46
47
48
49
50
51
52
53
54
55
56
57
58
59
60
61
62
63
64
65

```
GGGCCGAGGCCAACCGTTTCATAGAGTCGGTCCTGCCGACCCTGTGGATG
CTCAAGGACTACGCACTGCAAAGCGGTGCCGACTGGCCTTCGAACATCC
GGTCAGCAAACCGGTGGTTCTGACCAGCCGGGAGAAGGAAGTGTTCAGT
GGTGCGCCATCGGCAAGACCAGTTGGGAGATATCGGTTATCNTGCACTGC
TCGGAAGCCAATGTGAACTTCCATATGGGAAATATTCGGCGGAAGTTCGG
TGTGACCTCCCGCCGCGTAGCGCTGAGAGATCCCCTCATAATCCCCCAA
GCGTAACCATGTGTGAATAAATTTTGAGCTAATAGGGTTCAGCCACGAG
TAAGTCTTCCCTTTGTATTGTGTAACCAGAATGCCGCAAAACTTCCATGC
CTAAGCGAACTGTTGAAAGTACGTTTCGATTTCTGACTGTGTTAACCTGA
AAGTGCTTGGTCCCACCTTGTTCCTGAACATGAACGCCCCGCAAGCCAAC
ATGTTAGTTTGAAACTTCAGGGGAATTACCAACAGGAAATCATAAACGC
TCTGAACCTTGCTCGTTTGGGTTTGGGGGAAGGGCCTAATTTCCGGAGGG
CAGGAACTTTTTTCAGGTTTCGGGAAAGGGGGTTTTTTTTCAATTCTTTC
ATTTTTCCCTTCTTCAAAAAAAAAAATATTATAAAAAAAAAAAGTTTTGGTG
TGGGGGGGGGGTTTTGTTTAAATATTTTTTCTAACCAACGCGGGGAAAGA
AAATATTTTT
```

Note:
Highlight (yellow, 111-165): R0062, pLux promoter;
Highlight (blue, 174-185): B0034, Ribosome binding site;
Highlight (cyan, 192-872): C0079, LasR (part);
Highlight (pink, 873-1211): IS10 transposase (part);
CGCGTAGCG: target site for transposition.

LasR-C-Forward

Sequence: TGGGTCTTACTCTCTAA
Description: Forward, starting from the C terminal of LasR

Sequencing with LasR-C-Forward showed that the sequence remained as expected – terminator (red), pLux promoter (yellow), and GFP generator (green) from left to right – which shows the absence of mutation. Sequencing results are as follows:

```
> LasR-pLux-PF-LasRC-F 1345 ABI
1→
CGGGGGCTCAAATAAAACGAAAGGCTCAGTCGAAAGACTGGGCCTTTCGT
TTTATCTGTTGTTTGTTCGGTGAACGCTCTCTACTAGAGTCACACTGGCTC
ACCTTCGGGTGGGCCTTCTGCGTTTATA TACTAGAGACCTGTAGGATCG
TACAGGTTTACGCAAGAAAATGGTTTGTATAGTCGAATAAAATACTAGAG
TCACACAGGAAAGTACTAGATGCGTAAAGGAGAAGAACTTTTCACTGGAG
TTGTCCCAATTCTTGTGTAATTAGATGGTGATGTTAATGGGCACAAATTT
TCTGTCAGTGGAGAGGGTGAAGGTGATGCAACATACGAAAACCTTACCCT
TAAATTTATTTGCACTACTGGAAAACCTACCTGTTCCATGGCCAACACTTG
TCACTACTTTTCGGTTATGGTGTTCATGCTTTGCGAGATACCCAGATCAT
```

1
2
3
4
5
6
7
8
9
10
11
12
13
14
15
16
17
18
19
20
21
22
23
24
25
26
27
28
29
30
31
32
33
34
35
36
37
38
39
40
41
42
43
44
45
46
47
48
49
50
51
52
53
54
55
56
57
58
59
60
61
62
63
64
65

```
ATGAAACAGCATGACTTTTTCAAGAGTGCCATGCCCGAAGGTTATGTACA
GGAAAGAACTATATTTTTCAAAGATGACGGGAACTACAAGACACGTGCTG
AAGTCAAGTTTGAAGGTGATACCCTTGTTAATAGAATCGAGTTAAAAGGT
ATTGATTTTAAAGAAGATGGAAACATCTTGGACACAAATGGAATACAA
CTATAACTCACACAATGTATACATCATGGCAGACAAACAAAAGAATGGAA
TCAAAGTAACTTCAAAATTAGACACAACATGAAGATGGAAGCGTTCAA
CTAGCAGACCATTATCAACAAAATACTCCAATTGGCGATGGCCCTGTCCT
TTTACCAGACAACCATTACCTGTCCACACAATCTGCCCTTTCGAAAGATC
CCAACGAANAGAGAGACCACATGGTCCCTTCTTGAGTTTGTAACAGCTGCT
GGGATTACACATGGCATGGATGAACTATACAAATAATAACTAGAGCCA
GGCATCAAATAAAACGAAAGGCTCAGTCGAAAGACTGGGCCTTTCGTTTT
ATCTGTTGTTTGTGCGGTGAACGCTCTCTACTAGAGTCACACTGGCTCACC
TTCGGGTGGGCCTTTTCTGCGTTTATA TACTATTAGCGGGCGCTGCAGGC
TTCCTCGCTCACTGACTCCCCTGCGCCTCGGTGTTTCGGGCTGGCGGGA
AGCGGGTATCAGCTTCACTCCAAGGGGGGTAATACGGTTTTTCCCCC
AAAAATCCGGGGGATAAACACCCGGGAAAAAAAAAACTTGGTGAAACC
AAAAGGGGCCCCACAAAAAGGGGCCCGGGAAAACCCGGTAAAAAAA
AAGGGGCCCCCGGCGGTGTTGTTCTGGTGGTGGGGGTTTTTTTT
```

Note:

Highlight (red, 8-129): B0015, Terminator;
Highlight (yellow, 138-192): R0062, pLux promoter;
Highlight (green, 193-1077): E0240, GFP generator;

GFP-N-Reverse

Sequence: GTGCCATTAAACATCACCATC

Description: Reverse, starting at 55th bp from the N terminal of GFP

Sequencing with GFP-N-Reverse showed that the sequence was not the same as expected. From left to right, these results showed: part of GFP (green), pLux promoter (yellow), terminator (red), C terminal of LasR (cyan), and a new inserted sequence (pink). This new sequence was demonstrated to be part of an IS10 transposase gene according to BLASTn results from NCBI. The transposon target site is also marked (Bold black, highlighted pink). Sequencing results are as follows:

```
>LasR-pLux-PF-GFPN-R    1403    ABI
1→
GGGGGGGGGGTTGGAAAAGTTGCTTCTCCTTTACGCATCTAGTACTTTCC
TGTGTGACTCTAGTATTTATTCCCTTTTAGCAAACCATTTTCTTGCGTAA
ACCTGTACGATCCTACAGGTCTCTAGTATATAAACGCAGAAAGGCCACC
CGAAGGTGAGCCAGTGTGACTCTAGTAGAGAGCGTTCACCGACAAACAAC
AGATAAAACGAAAGGCCAGTCTTTCGACTGAGCCTTTCGTTTTATTGA
TGCCTGGCTCTAGTATTATTAGAGAGTAATAAGACCCAAATTAACGGCCA
```

1
2
3
4
5
6
7
8
9
10
11
12
13
14
15
16
17
18
19
20
21
22
23
24
25
26
27
28
29
30
31
32
33
34
35
36
37
38
39
40
41
42
43
44
45
46
47
48
49
50
51
52
53
54
55
56
57
58
59
60
61
62
63
64
65

```
TAATGGCCGCTACGCGCTGATGAATCCCCTCATGATTTTCGGCAAAAATCA  
TTAATGTGAGGTGGATACTTGTCTTGCCAGATGATCAAATGGTTTCGCGT  
AAACTCTTGAATCAGACCACATGATGTGCGATCTCGATATTTTACATCAC  
TCTCTTTAAGAATTCTGCCCTGAATTACAGTTAGAACGACTCAACAGCTG  
AACGTTGCGCTTGTACGCCTTACTTGAGTGTAACACTCTCACTCTTACC  
GAAATGGTTCGTAACCTGACAACCTAAGTGAGATCAAAACATAACATCAA  
ACGACTCGACGGATTGGTATGTAATCGTCACCTCCGCAAAGAGCGACTCG  
CTGTATACCGTTGGCCTGCTATCTATATCTGTTTCGGGCAATACGATGCC  
ATTGTAGTTGGTGACTGGTCTGATATTCGAGAGCCTAAACAACCTTATCGT  
GGTTGCGAGCTTCAGTCGCACTACCTGGTCGTTCTGATACTCTTTATGAG  
AAAGCGTTCATCTTCCGATCTTATGCTCAAGAAAGCTCATGATCATT  
TCTAGCCGATCTTGTGATAGGTCATCGGAGAACTCCACTCTCGCTCATT  
GTCAGGGATGTGGGCTTTTAAAGGGACGTGGTATAATCCCTTGGAAAATTT  
GGGTAGGTACTGGGTTACTCGAAGAGGAAGGAAAATTTTATATGCGGGAC  
CTTAGGAAGGGAAAACCGGGAAACCATTACAGCACTTAACTGTTTTTTGT  
TCTCTATACCCCTCCAAAATTTTGGTGTTTAAAAGTGTTTAATTA  
AATCCAATTTCTAGTGCAAATGTCGTTTTTAAAAAATTTCTTTTGTCTAA  
GGGCTGAAGAAATTTGACCTTTCTGCAGGGGAAACCTTTTGTCTCACCG  
CCCAGCAATTTAAAAACTTTCTTTCTGCACGGGTGGGGCAGGGGAGACCC  
GGGAGGTCCCTTTTTTCCACCTAACTTTTTTCGCCTGTTGTTAAAAAATTAC  
AAAACACACCCCTACCAAATCTCTTTTTTATAAAATTTACCTCCTTCTTA  
GGAATAGCCCGAGAGTAGGCCAAAAAATATATTA  
TAAAAAATTAACAC  
TCT
```

Note:

- Highlight (green, 14-57): E0240, GFP generator (N terminal);
- Highlight (yellow, 66-120): R0062, pLux promoter;
- Highlight (red, 129-257): B0015, Terminator;
- Highlight (cyan, 266-307): C0079, LasR (C terminal);
- CGCTACGCG**: target site for transposition (duplication).
- Highlight (pink, 317-1038): IS10 transposase (part);

BB-C-Reverse

Sequence: AATACCGCCTTTGAGTGAGC

Description: Reverse, starting from the C terminal of MCS on the plasmid

Sequencing with BB-C-Reverse verified the GFP generator (green) and pLux promoter (yellow), which indicate a lack of mutation. Sequencing results are as follows:

```
> LasR-pLux-PF-BBR      1382      ABI  
1→  
GGGCGCCATCGTACGACCGAGCGCAGCGAGTCAGTGAGCGAGGAAGCCTG
```

1
2
3
4
5
6
7
8
9
10
11
12
13
14
15
16
17
18
19
20
21
22
23
24
25
26
27
28
29
30
31
32
33
34
35
36
37
38
39
40
41
42
43
44
45
46
47
48
49
50
51
52
53
54
55
56
57
58
59
60
61
62
63
64
65

```
CAGCGGCCGCTACTAGTATATAAACGCAGAAAGGCCACCCGAAGGTGAG  
CCAGTGTGACTCTAGTAGAGAGCGTTCACCGACAAACAACAGATAAAACG  
AAAGGCCAGTCTTTTCGACTGAGCCTTTTCGTTTTATTTGATGCCTGGCTC  
TAGTATTATTATTTGTATAGTTCATCCATGCCATGTGTAATCCCAGCAGC  
TGTTACAAACTCAAGAAGGACCATGTGGTCTCTCTTTTCGTTGGGATCTT  
TCGAAAGGGCAGATTGTGTGGACAGGTAATGGTTGTCTGGTAAAAGGACA  
GGGCCATCGCCAATTGGAGTATTTTGTGATAATGGTCTGCTAGTTGAAC  
GCTTCCATCTTCAATGTTGTGTCTAATTTTGAAGTTAACTTTGATTCCAT  
TCTTTTGTGTCTGCCATGATGTATACATTGTGTGAGTTATAGTTGTAT  
TCCAATTTGTGTCCAAGAATGTTTCCATCTTCTTTAAAATCAATACCTTT  
TAACTCGATTCTATTAACAAGGGTATCACCTTCAAACCTGACTTCAGCAC  
GTGTCTTGTAGTTCCTCGTCATCTTTGAAAAATATAGTTCTTTCCTGTACA  
TAACCTTCGGGCATGGCACTCTTGAAAAAGTCATGCTGTTTCATATGATC  
TGGGTATCTCGCAAAGCATTGAACACCATAACCGAAAGTAGTGACAAGTG  
TTGGCCATGGAACAGGTAGTTTTCCAGTAGTGCAAATAAATTTAAGGGTA  
AGTTTTCCGTATGTTGCATCACCTTCACCCTCTCCACTGACAGAAAATTT  
GTGCCATTAACATCACCATCTAATTCAACAAGAATTGGGACAACCTCCAG  
TGAAAAGTTCTTCTCTTTACGCATCTAGTACTTTCTGTGTGACTCTAG  
TATTTATTCGACTATAACAAACCATTTTCTTGCCTAAACCTGTACGATCC  
TACAGGCTCTCTAGTATATAAACGCAAAAAGGGCCACCCCGAAGGGTGAGC  
CAGTGTGACTCTAATAGAGAGCGGTCACCGACAAACAACAGAAAAAACG  
AAAGGCCAGTCTTTTCGAACGGAACCTTTTCGTTTTAATTTGAATGCCT  
GGGTCTTAATATTTATTTAAAAAAGAAAAAGAAACCAAAATTTTACGG  
GCCATAAGGGGGCCGCCCTCCCCCGCGGAAGAAAACCCCCCAAGAG  
AAATTTTGGGTAAAAAACAATTTTAAAGTTTAAAGGGGGGGGAAAA  
CACACCCCTCCTTGTGTCTCAAATAAGATATATAAAAAAGGGGGGGTT  
TTTTTCGCCCGCAAAAAAATAAAAAA
```

Note:
Highlight (green, 69-944): E0240, GFP generator;
Highlight (yellow, 953-1007): R0062, pLux promoter;

GFP-C-Forward

Sequence: GGCATGGATGAACTATACAAATAA
Description: Forward, starting from the C terminal of GFP

Sequencing with GFP-C-Forward showed that the sequence was the same as expected – terminator (red), and pSB1A3 backbone (light grey) – which indicated a lack of mutation. Sequencing results are as follows:

```
> LasR-pLux-PF-GFPC-F 1334 ABI  
1→  
AGGAGCCAGGGCATCAATAAAACGAAAGGCTCAGTCGAAAGACTGGGCCT
```

1 TTCGTTTTATCTGTTGTTTGTTCGGTGAACGCTCTCTACTAGAGTCACACT
2 GGCTCACCTTCGGGTGGGCCTTTCTGCGTTTATA TACTAGTAGCGGCCGC
3 TGCAGGCTTCCTCGCTCACTGACTCGCTGCGCTCGGTTCGGCTGCGG
4 CGAGCGGTATCAGCTCACTCAAAGCGGTAATACGGTTATCCACAGAATC
5 AGGGGATAACGCAGGAAAGAACATGTGAGCAAAGGCCAGCAAAGGCCA
6 GGAACCGTAAAAAGGCCGCGTTGCTGGCGTTTTTCCACAGGCTCCGCCCC
7 CCTGACGAGCATCACAAAAATCGACGCTCAAGTCAGAGGTGGCGAAACCC
8 GACAGGACTATAAAGATAACCAGGCGTTTCCCCCTGGAAGCTCCCTCGTGC
9 GCTCTCCTGTTCCGACCCTGCCGCTTACCGGATACCTGTCCGCCTTTCTC
10 CCTTCGGGAAGCGTGGCGCTTTCTCATAGCTCACGCTGTAGGTATCTCAG
11 TTCGGTGTAGGTCGTTGCTCCAAGCTGGGCTGTGTGCACGAACCCCCCG
12 TTCAGCCCGACCGCTGCGCCTTATCCGGTAACTATCGTCTTGAGTCCAAC
13 CCGGTAAGACACGACTTATCGCCACTGGCAGCAGCCACTGGTAACAGGAT
14 TAGCAGAGCGAGGTATGTAGGCGGTGCTACAGAGTTCTTGAAGTGGTGGC
15 CTAACACTACGGCTACACTAGAAGAACAGTATTTGGTATCTGCGCTCTGCTG
16 AAGCCAGTTACCTTCGGAAAAAGAGTTGGTAGCTCTTGATCCGGCAAACA
17 AACCACCGCTGGTAGCGGTGGTTTTTTTTGTTTGCAAGCAGCAGATTACGC
18 GCAGAAAAAAAGGATCTCAAGAAGATCCTTTGATCTTTTCTACGGGGTCT
19 GACGCTCAGTGGAACGAAAACCTCACGTTAAGGGATTTTGGTCATGAGATT
20 ATCAAAAAGGATCTTCACCTAGATCCTTTTAAATAAAAAATGAAGTTTTA
21 AATCAATCTAAAGTATATATGAAGTAAACTTGGTCTGACAGTTACCAATG
22 GCTTAATCAGTGAGGCACCTTATCTCAACGGATCTGTCTTATTTTCGTTCA
23 TCCCATAAATTGGCCTGAACTCCCCCGTCCGTGGAAAAAAAACCTTACAAA
24 CCGGGGGGGGGGCTTTACCCATTTCGGGGGCCCCCAGGGGGGGTGCCAAG
25 GGAGAAAACCCCGCGCAAAAAACCCCCCGCCCCCCCCCGGGGGGCCTC
26 CCCAAAAAAATTTTTATTATTTAACACCCAAAA

Note:

Highlight (red, 6-134): B0015, Terminator;
Highlight (light grey, 151-1182): pSB1A3, vector backbone (part).

Supplemental References:

1
2
3
4 Bakshi, S., Siryaporn, A., Goulian, M., and Weisshaar, J.C. (2012). Superresolution imaging of
5 ribosomes and RNA polymerase in live *Escherichia coli* cells. *Mol. Microbiol.* 85, 21 – 38.
6

7
8 Basu, S., Gerchman, Y., Collins, C.H., Arnold, F.H., and Weiss, R. (2005). A synthetic
9 multicellular system for programmed pattern formation. *Nature* 434, 1130 – 1134.
10

11
12 Craig, N.L. (2002). *Mobile DNA II* (ASM Press).
13

14 Danino, T., Mondragón-Palomino, O., Tsimring, L., and Hasty, J. (2010). A synchronized quorum
15 of genetic clocks. *Nature* 463, 326 – 330.
16

17
18 Ellis, T., Wang, X., and Collins, J.J. (2009). Diversity-based, model-guided construction of
19 synthetic gene networks with predicted functions. *Nat. Biotechnol.* 27, 465 – 471.
20

21
22 Gillespie, D.T. (1977). Exact stochastic simulation of coupled chemical reactions. *J. Phys. Chem.*
23 81, 2340 – 2361.
24

25
26 Milo, R., Jorgensen, P., Moran, U., Weber, G., and Springer, M. (2010). BioNumbers--the
27 database of key numbers in molecular and cell biology. *Nucleic Acids Res.* 38, D750 – 753.
28

29
30 Sayut, D.J., and Sun, L. (2010). Slow activator degradation reduces the robustness of a coupled
31 feedback loop oscillator. *Mol. Biosyst.* 6, 1469 – 1474.
32

33
34 Sousa, A., Bourgard, C., Wahl, L.M., and Gordo, I. (2013). Rates of transposition in *Escherichia*
35 *coli*. *Biol. Lett.* 9, 20130838.
36

37
38 Wu, M., Su, R.-Q., Li, X., Ellis, T., Lai, Y.-C., and Wang, X. (2013). Engineering of regulated
39 stochastic cell fate determination. *Proc. Natl. Acad. Sci. U. S. A.* 110, 10610 – 10615.
40

41
42 Zhou, J.X., Aliyu, M.D.S., Aurell, E., and Huang, S. (2012). Quasi-potential landscape in complex
43 multi-stable systems. *J. R. Soc. Interface R. Soc.* 9, 3539 – 3553.
44
45
46
47
48
49
50
51
52
53
54
55
56
57
58
59
60
61
62
63
64
65